

1 **Global ecological and biogeochemical impacts of pelagic tunicates**

2

3

4 Jessica Y. Luo¹, Charles A. Stock¹, Natasha Henschke², John P. Dunne¹, Todd D. O'Brien³

5

6 ¹NOAA Geophysical Fluid Dynamics Laboratory, 201 Forrestal Rd, Princeton NJ 08540

7 ²School of Biological, Earth and Environmental Sciences, University of New South Wales,
8 Sydney, NSW 2052

9 ³NOAA NMFS Office of Science and Technology, Silver Spring MD, USA

10

11 Manuscript correspondence: Jessica.Luo@noaa.gov

12

13

14 Keywords: gelatinous zooplankton, pelagic tunicates, ocean biogeochemical cycles, carbon
15 export, global model

16 **Abstract**

17

18 The pelagic tunicates, gelatinous zooplankton that include salps, doliolids, and appendicularians,
19 are filter feeding grazers thought to produce a significant amount of particulate organic carbon
20 (POC) detritus. However, traditional sampling methods (i.e., nets), have historically
21 underestimated their abundance, yielding an overall underappreciation of their global biomass
22 and contribution to ocean biogeochemical cycles relative to crustacean zooplankton. As climate
23 change is projected to decrease the average plankton size and POC export from traditional
24 plankton food webs, the ecological and biogeochemical role of pelagic tunicates may increase;
25 yet, pelagic tunicates were not resolved in the previous generation of global earth system climate
26 projections. Here we present a global ocean study using a coupled physical-biogeochemical
27 model to assess the impact of pelagic tunicates in the pelagic food web and biogeochemical
28 cycling. We added two tunicate groups, a large salp/doliolid and a small appendicularian to the
29 NOAA-GFDL Carbon, Ocean Biogeochemistry, and Lower Trophics version 2 (COBALTv2)
30 model, which was originally formulated to represent carbon flows to crustacean zooplankton.
31 The new GZ-COBALT simulation was able to simultaneously satisfy new pelagic tunicate
32 biomass constraints and existing ecosystem constraints, including crustacean zooplankton
33 observations. The model simulated a global tunicate biomass of 0.10 Pg C, annual production of
34 0.49 Pg C y⁻¹ in the top 100 m, and export flux of 0.7 Pg C y⁻¹, representing 11% of the total
35 export flux past 100 m. Overall export from the euphotic zone remained largely constant, with
36 the GZ-COBALT pe-ratio only increasing 5.3% (from 0.112 to 0.118) compared to the
37 COBALTv2 control. While the bulk of the tunicate-mediated export production resulted from the
38 rerouting of phytoplankton- and mesozooplankton-mediated export, tunicates also shifted the
39 overall balance of the upper oceans away from recycling and towards export. Our results suggest
40 that pelagic tunicates play important trophic roles in both directly competing with
41 microzooplankton and indirectly shunting carbon export away from the microbial loop.

42 1. Introduction

43

44 In recent decades, there has been a growing recognition of the prevalence and ecological
45 importance of gelatinous zooplankton (GZ), which include the cnidarian jellyfish, ctenophores,
46 and pelagic tunicates (Hays et al., 2018; Henschke et al., 2016). While they have been a natural
47 component of marine ecosystems extending back to the Cambrian (Hagadorn et al., 2002), their
48 abundance and distributions have been largely overlooked among the public and non-GZ
49 specialists (Condon et al., 2012). This may be due to a combination of the erroneous perception
50 of GZ being “trophic dead-ends” within marine food webs (Hays et al., 2018; Lynam et al.,
51 2006; Verity and Smetacek, 1996), as well as systematic biases in sampling leading to overall
52 under-sampling of their biomass. Net-based sampling has been prevalent for over a century, and
53 is very effective for sampling fish and hard-bodied, crustacean zooplankton (Wiebe and
54 Benfield, 2003). Unfortunately, the fragile gelatinous zooplankton are often broken apart in nets,
55 yielding a *ca.* 3 fold underestimation of their abundance and a *ca.* 10 fold (range: 5-15)
56 underestimation of their carbon biomass relative to non-extractive, optical sampling (Remsen et
57 al., 2004). The rise of in-situ plankton imaging systems have resulted in improved estimates of
58 GZ abundance and distribution (e.g., Luo et al., 2014), yielding advances in understanding of
59 their food-web interactions and biogeochemical impacts (Greer et al., 2021; Robison, 2005;
60 Smith Jr et al., 2014). Combined with the increase in ecosystem-level studies of GZ (e.g., Stukel
61 et al., 2021) and technological advances revealing the importance of GZ as food for higher
62 trophic levels (Hays et al., 2018), there has been an overall paradigm shift in our understanding
63 of the importance and role of gelatinous zooplankton within marine ecosystems.

64 Amongst zooplankton, GZ are notable for their high clearance rates and boom-and-bust
65 population dynamics, which yield mass mortality events (“jelly-falls”) that sink rapidly through
66 the water column (Acuña et al., 2011; Billett et al., 2006; Lebrato et al., 2012; Lucas and
67 Dawson, 2014). As a result, models have estimated, based on population densities and allometric
68 scaling of ecological and physiological rates, a large contribution (e.g., 1.6-5.2 Pg C y⁻¹ in Luo et
69 al. 2020) of GZ-mediated carbon in the global biological pump, with their relative impact
70 increasing with depth (Lebrato et al., 2019; Luo et al., 2020). However, these studies have been
71 done independently of other biogeochemical and ecological constraints (i.e., “offline”
72 calculations), which may yield unrealistic estimates of GZ contributions to marine ecosystems.
73 Indeed, in a new model that includes cnidarian jellyfish as a plankton functional type
74 (PlankTOM11), global export production exhibited very modest increases (+0.1 Pg C y⁻¹),
75 suggesting that the online inclusion of a jellyfish class does not by itself substantially increase
76 total export production (Wright et al., 2021). Of the three major groups of GZ considered by Luo
77 et al. (2020), cnidarian jellyfish had the largest standing stock biomass but pelagic tunicates,
78 despite their much lower biomass, over two times more sinking detritus than cnidarians and
79 ctenophores combined.

80 These pelagic tunicates, small filter-feeders including appendicularians, salps, doliolids,
81 and pyrosomes, are less conspicuous than the cnidarians and ctenophores, but are highly
82 significant components of marine ecosystems due to their low trophic position, high clearance
83 rates, and fast sinking fecal pellets (Andersen, 1998; Berline et al., 2011; Henschke et al., 2016;
84 Hopcroft and Roff, 1998). Compared to crustacean mesozooplankton such as copepods which
85 feed at predator to prey size ratios ranging from 5:1 to 100:1 (Hansen et al., 1994), pelagic
86 tunicates can feed at predator to prey size ratios ranging from 10:1 to 10000:1 (Conley et al.,
87 2018). Salps pump water through their fine mucous meshes that can filter submicron particles

88 such as bacteria and picoplankton; they are able to sustain the entirety of their energetic demands
89 by grazing on these size classes alone (Sutherland et al., 2010). Using both external and internal
90 filters to feed, appendicularians have the widest range of predator to prey size ratios (exceeding
91 2500:1 to lower than 10:1), and thus can feed on organisms ranging from 0.2-20 μm in size
92 (Conley et al., 2018; Deibel and Lee, 1992; Fernández et al., 2004). The offline Luo et al. (2020)
93 model estimated that, due to these feeding characteristics, these pelagic tunicates consume
94 between 3.8-8.3 Pg C y^{-1} in prey. Of this consumption, approximately 12-17% were later
95 consumed by higher trophic level predators, and 55-60% became detritus.

96 Global ocean biogeochemical and marine ecosystem models typically represent marine
97 food webs with roughly linear food chains of phytoplankton to zooplankton to (implicit) fish
98 (Kearney et al., 2021). The traditional inclusion of multiple zooplankton groups has been to
99 distinguish between zooplankton size, such as microzooplankton and mesozooplankton, with the
100 latter parameterized using crustacean zooplankton measurements (Aumont et al., 2015;
101 Buitenhuis et al., 2006; Stock and Dunne, 2010; Ward et al., 2012). Even in models with
102 complex food-webs, predator to prey size ratios beyond $\sim 50:1$ (c.f. Hansen et al., 1994) are
103 rarely considered. As such, current ocean biogeochemical models typically represent a marine
104 ecosystem in which crustaceans dominate zooplankton ecology. While this view represents
105 certain ecosystems well (Pershing and Stambieskin, 2020), globally, there is a tension between
106 the traditional, crustacean-dominated zooplankton view of marine ecosystems and a shifting
107 paradigm that emphasizes the role of GZ. Unfortunately, GZ-focused offline models are unable
108 to reconcile this tension, as evidenced by high GZ-mediated global ingestion and production
109 rates (Luo et al., 2020) that may not support primary and secondary production rates for
110 crustacean zooplankton consistent with observations. Additionally, offline studies are limited in
111 the capacity to explore factors underlying observed GZ niches, and how GZ impacts emergent
112 food web patterns. These challenges are compounded by stubborn limitations in GZ observations
113 which are patchy and inconsistently sampled.

114 In this study, we added two explicit zooplankton functional types that represent
115 thaliaceans (salps, doliolids, pyrosomes) and appendicularians into Carbon, Ocean
116 Biogeochemistry, and Lower Trophics version 2 (COBALTv2; Stock et al., 2020), a global
117 model designed to represent a “traditional” marine ecosystem dominated by crustacean
118 zooplankton. We ask the following four questions:

119 1) Can simulations capture the magnitude and gradients of observed GZ biomass across
120 ocean biomes and along productivity gradients, after accounting for approximately an order of
121 magnitude under-sampling by nets?

122 2) Can simulations reconcile recent evidence for the importance of GZ with established
123 evidence for the prominence of crustacean zooplankton in biogeochemical cycles and the
124 plankton food web?

125 3) How does a simulation of GZ-modulated export that satisfies multiple food web
126 constraints compare with offline estimates?

127 4) What is the net impact of GZ zooplankton on the partitioning of carbon flows between
128 recycling, carbon export and energy flows to higher trophic levels?

129

130 2. Methods

131

132 As a brief overview of the methods, we begin with a description of plankton food web dynamics
133 within the original COBALTv2 marine ecosystem model (Stock et al., 2014a, 2020), followed by
134 the GZ additions that comprise GZ-COBALT: small and large pelagic tunicates. We first
135 describe the baseline parameterization of GZ-COBALT, and then a few sensitivity experiments
136 that explore parts of the parameter space and particular elements of the tunicate groups that make
137 them distinct from crustacean zooplankton. Next, we detail the physical framework of the model.
138 Finally, we describe the construction of a validation dataset for the two new GZ groups and the
139 identification of an emergent relationship that contrasts gelatinous against crustacean
140 zooplankton. The model is validated against multiple constraints, comprising new and
141 established ecological and biogeochemical datasets.

142

143 2.1 COBALT Ecosystem Model

144

145 We use the COBALTv2 marine ecosystem model (Stock et al., 2020) as our baseline
146 model configuration, with slight modifications. COBALTv2 is a 33-tracer, intermediate
147 complexity model, representing biogeochemical cycles of carbon, alkalinity, oxygen, nitrogen,
148 phosphorus, iron, silica, calcium carbonate, and lithogenic materials. The food web consists of
149 three phytoplankton and three zooplankton functional types, as well as a free-living heterotrophic
150 bacteria group. Two phytoplankton size classes (small and large) are represented, as well as
151 diazotrophs, parameterized as a large *Trichodesmium* group. The small phytoplankton type
152 includes cyanobacteria and other phytoplankton, up to 10 μm in equivalent spherical diameter
153 (ESD), and the large phytoplankton type represents diatoms and other large phytoplankton from
154 10-100 μm in ESD. The different sized phytoplankton are parametrized to capture size-based
155 contrasts in nutrient uptake, light harvesting, carbon to chlorophyll ratios, and susceptibility to
156 microzooplankton grazing (Edwards et al., 2015, 2012; Hansen et al., 1994; Munk and Riley,
157 1952), such that the small phytoplankton are more successful in the low nutrient, seasonally
158 stable subtropical gyres, and large phytoplankton are more competitive in the highly seasonal,
159 high nutrient oceans (Stock et al., 2014a, 2020).

160 The base configuration of COBALTv2 contains three zooplankton size classes: a
161 microzooplankton and two size classes of crustacean mesozooplankton. Microzooplankton ($<$
162 200 μm ESD) include ciliates and heterotrophic nanoflagellates, medium zooplankton (i.e, small
163 mesozooplankton; 200-2000 μm ESD) represent small to medium-bodied copepods, and large
164 zooplankton (2 – 20 mm ESD) represent large copepods and krill (Stock et al., 2014a). Predator-
165 prey relationships are also largely based on size, with microzooplankton predating on bacteria
166 and small phytoplankton, small mesozooplankton predating on diazotrophs, large phytoplankton,
167 and microzooplankton, and large mesozooplankton predating on diazotrophs, large
168 phytoplankton, and small mesozooplankton (Fig. 1a). Grazing is modeled as a Hollings Type II
169 function with density-dependent switching (Stock et al., 2008), with maximum biomass specific
170 grazing rates decreasing with increasing zooplankton size (Hansen et al., 1997). Grazing half-
171 saturation constants do not vary between the zooplankton classes, and are tuned to reproduce
172 observed patterns in phytoplankton biomass and turnover rates (Stock and Dunne, 2010).

173 Zooplankton grazing was assimilated at an assimilation efficiency (AE) of 0.7, with the
174 non-assimilated grazing partitioned into dissolved and particulate (detritus) matter, depending on
175 size. Detritus partitioning of non-assimilated matter were: 1/6 for microzooplankton, 2/3 for

176 medium, and 1 for large zooplankton, and the remainder separated between labile (70%), semi-
 177 labile (20%) and semi-refractory (10%) dissolved matter. Assimilated matter was partitioned into
 178 respiration (basal and active) and zooplankton production. Basal respiration is proportional to
 179 biomass, whereas active respiration is proportional to ingestion rates. When respiration rates
 180 exceed assimilated ingestion, production becomes negative and re-contributes to zooplankton
 181 mortality. The temperature dependence of biological rates (phytoplankton nutrient uptake and
 182 growth, zooplankton grazing) is determined by a common Eppley (1972) curve with a Q_{10} factor
 183 of 1.88, representing a near doubling of rates for every 10°C temperature increase.

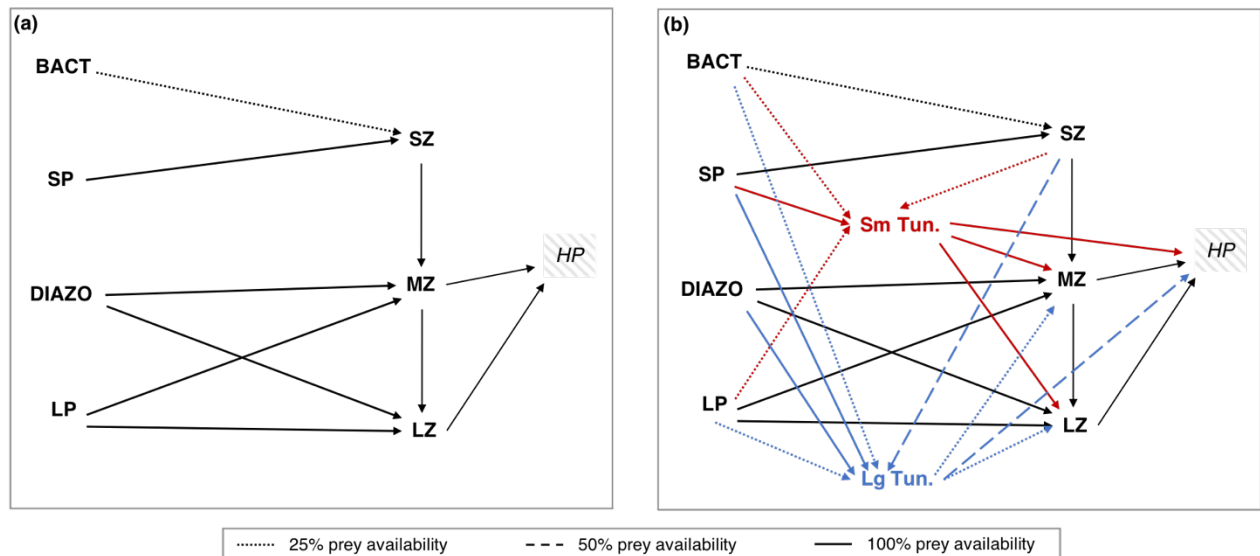
184
 185

186 2.2 Gelatinous Zooplankton in COBALT (GZ-COBALT)

187

188 Following Luo et al. (2020), we introduced two new pelagic tunicate groups into
 189 COBALTv2 (Fig. 1b): small tunicates, which represents Appendicularians, and large tunicates,
 190 which represents Thaliaceans (i.e., salps and doliolids). Appendicularians are small, free-
 191 swimming organisms that produce gelatinous houses for filter-feeding, which are discarded when
 192 clogged and re-created multiple times per day. Salps and doliolids are also filter-feeders, but
 193 unlike appendicularians, are colonial (though salps and doliolids have solitary life stages), form
 194 rapidly sinking fecal pellets (Perissinotto and Pakhomov, 1998), and exhibit mass die-offs (jelly-
 195 falls; Henschke et al., 2013).

196



197

198 **Figure 1.** Food web structure of (a) COBALTv2 base model, and (b) GZ-COBALT model. Additional functional
 199 groups in GZ-COBALT include a small and large tunicate. Bact = free living bacteria, SP = small phytoplankton,
 200 Diazo = diazotrophs, LP = large phytoplankton, SZ = small zooplankton, MZ = medium zooplankton, LZ = large
 201 zooplankton, and HP = higher trophic-level predators. Note that within typical zooplankton size categories, small
 202 zooplankton would be considered microzooplankton, and medium and large zooplankton would be considered
 203 mesozooplankton.

204

205 2.2.1 GZ food web structure

206

The pelagic tunicates were inserted into the COBALTv2 model as summarized in Fig. 1.

207

Pelagic tunicates have the widest prey-to-predator size ratios among zooplankton (Conley et al.,
 208 2018), with appendicularians preying on organisms ranging from 0.04 – 20% of its size,

209 equivalent to 0.2 – 20 μm in length (Deibel and Lee, 1992; Fernández et al., 2004; Lombard et
210 al., 2011). Small tunicates in the baseline model setting are thus able to consume bacteria, small
211 phytoplankton, large phytoplankton, and microzooplankton. This is consistent with previous
212 efforts that included appendicularians in a NPZD-type model (Berline et al., 2011) wherein small
213 tunicates consumed small phytoplankton, which lie near the center of their prey kernel, with high
214 preference (100% prey availability), and all others with low preference (25% prey availability).
215 Appendicularians are important prey for many invertebrates and fish, often contributing large
216 proportions of the diets of medusae jellyfish and many larval fish species (Gorsky and Fenaux,
217 1998; Llopiz et al., 2010; Purcell et al., 2005). Thus, small tunicates were predated upon by
218 medium and large zooplankton and higher trophic level predators with high preference (Fig. 1b).

219 While they have relatively large body sizes (e.g., the solitary form of *Salpa thompsoni*
220 can exceed 10 cm; Dubischar et al., 2006), salps have fine mucous meshes that can filter
221 submicron particles, and have a preference for grazing on small algae such as picoplankton
222 (Sutherland et al., 2010). Salps are able to consume diatoms and bacteria, but with relatively low
223 efficiency (Dadon-Pilosof et al., 2019) and with many diatoms passing through salp guts
224 undigested (Harbison et al., 1986). Additionally, salps have been shown to be dominant grazers
225 on *Trichodesmium* in certain regions (Post, 2002). While, the prey of doliolids is less studied,
226 Walters et al. (2019) found using genetic approaches that doliolids preferentially consume
227 diatoms (particularly in their early life stages) and ciliates. Thus, in the present model, the large
228 tunicates were able to feed on small phytoplankton and diazotrophs with high preference (100%
229 prey availability), microzooplankton at medium preference (50% prey availability), and bacteria
230 and large phytoplankton at low preference (25% prey availability).

231 Large tunicate predators and parasites were traditionally thought to be primarily
232 saphirinid copepods and large hyperiid amphipods, including the predatory and parasitic
233 *Phronima* spp., which consume salp tissue and live in their cleared-out barrels (Laval, 1980;
234 Madin and Harbison, 1977; Takahashi et al., 2013). Restricted emphasis on these relatively rare
235 crustacean predators and parasites has yielded the misconception of gelatinous zooplankton,
236 particularly salps, as trophic dead-ends. However, increasing evidence has highlighted the role of
237 thaliaceans as food for fish and other higher trophic levels. Over 200 species of fish, turtles,
238 corals, and echinoderms consume salps, doliolids, and pyrosomes, with many predators filling
239 their guts with thaliaceans during bloom periods (Harbison, 1998; Henschke et al., 2016;
240 Mianzan et al., 2001). Therefore, in our model, large tunicates are predated upon by medium and
241 large zooplankton at low preference (25% prey availability), reflecting the specialized nature of
242 the copepod and amphipod predators relative to the broader crustacean zooplankton population,
243 and by higher trophic level predators at medium preference (50% prey availability).

244 The diets of small and large tunicates are fairly similar in the model, as they are both
245 microphagous generalists. Notably, there was no size scaling in the tunicates' diets relative to
246 their body size (i.e., smaller tunicates did not consume smaller prey), which is in contrast to
247 crustacean mesozooplankton; large tunicates have larger predator-to-prey size ratios than small
248 tunicates (Conley et al., 2018). Rather, the key distinction (with respect to food web dynamics)
249 between the tunicates is the level of predation. Small tunicates have very strong levels of top-
250 down control, exerted by all mesozooplankton and higher trophic level predators. While large
251 tunicates experience predation by similar predators as small tunicates in the model, the strength
252 of that predation is reduced to account for their larger size. Other distinctions between the two
253 tunicates, including ingestion rates, metabolic scalings, and susceptibility to jelly-falls are
254 described in the next sections.

255

256 2.2.2 Ingestion and assimilation

257 As filter feeders, the prey consumption rates of pelagic tunicates are typically measured
258 as biomass-specific clearance (or filtration) rates, yielding ingestion rates (I , $\text{mg C m}^{-3} \text{ d}^{-1}$) as the
259 product of the specific clearance rate (C_b , $\text{m}^3 \text{ mg C}^{-1} \text{ d}^{-1}$), prey biomass (P , mg C m^{-3}), and
260 predator biomass (Z , mg C m^{-3}) (Acuña et al., 2011):

$$261 \quad I = C_b P Z \quad (\text{eq. 1})$$

262 In contrast, COBALTv2 and other NPZD-type models utilize saturating functional response
263 (Hollings Type II in the case of one prey) for zooplankton grazing (Fasham et al., 1990;
264 Gentleman et al., 2003; Stock and Dunne, 2010):

$$265 \quad I = \frac{I_{\max} P Z}{K_i + P} \quad (\text{eq. 2})$$

266 Where I_{\max} is the maximum specific ingestion rate (d^{-1}), and K_i is the ingestion half-saturation
267 constant (mg C m^{-3}). At $K_i \gg P$, eq. (2) reduces to $I = (I_{\max}/K_i) * P * Z$, and C_b becomes equivalent
268 to I_{\max}/K_i (Acuña and Kiefer, 2000).

269 For small tunicate clearance rates, we used allometric relationships from Lombard et al.
270 (2009), which measured physiological rates for a common appendicularian, *Oikopleura dioica*.
271 Using a characteristic individual body size of 1 mm and associated biomass of $6.68 \mu\text{g C}$,
272 specific filtration rates at 0°C (converted using a Q10 of 1.88) range from 0.010-0.017 (mean:
273 0.013) $\text{m}^3 \text{ mg C}^{-1} \text{ d}^{-1}$ (Lombard et al., 2009a). Considering that the clearance rates of both small
274 and large tunicates do not significantly change with low to medium food concentrations (Gibson
275 and Paffenhöfer, 2000; Paffenhöfer and Köster, 2011), we opted for a higher tunicate half-
276 saturation constant ($K_i = 250 \text{ mg C m}^{-3}$) than that of crustacean zooplankton (102 mg C m^{-3} ;
277 Table 1), consistent with the estimated range of K_i for *O. dioica* of 20-500 mg C m^{-3} (Acuña and
278 Kiefer, 2000). The equivalent I_{\max} at low prey concentrations would be 2.50-4.25 (mean: 3.25) d^{-1} .
279 Following model tuning, we used an I_{\max} value on the low end of the range (1.875 d^{-1}) given a
280 mean K_i , to avoid overconsumption by small tunicates. However, considering the wide variation
281 in K_i , these values were well within the observational bounds. The tradeoffs between tunicates
282 and crustacean zooplankton were visualized in a plot of specific ingestion at 25°C (Fig. 2a): the
283 small tunicate I_{\max} and K_i results in a specific ingestion in between small/micro-zooplankton and
284 medium/crustacean zooplankton. Additionally, a sensitivity run was conducted to illustrate the
285 effect of the I_{\max} tuning choice (Section 2.3).

286 For large tunicates, we were able to use an allometric scaling relationship from a prior
287 effort (Luo et al., 2020) that compiled length, carbon biomass, and clearance rate relationships
288 from various studies (see Madin and Deibel, 1998) into a single equation. Using a characteristic
289 biomass of 1.5 mg C , which corresponds to a 20-38 mm length individual, specific clearance
290 rates at 0°C range from $4.2\text{E-}4$ to $7.4\text{E-}3$ (mean: $1.8\text{E-}3$) $\text{m}^3 \text{ mg C}^{-1} \text{ d}^{-1}$. Using a K_i of 250 mg C
291 m^{-3} , and the same relationship between clearance rates, K_i , and I_{\max} as above, we estimated large
292 tunicate I_{\max} values to be between 0.105-1.85 d^{-1} . In the model, we used a value in the lower half
293 of the reported range (0.55 d^{-1}), tuned in conjunction with other variables with wide uncertainty
294 bounds to match observed biomass concentrations. At the lowest prey concentrations, the I_{\max}/K_i
295 of large tunicates matched that of the large crustacean zooplankton. As prey concentrations
296 increased, large tunicate ingestion fell between that of the medium and large crustacean
297 zooplankton and reached its maximum ingestion rate much slower than either crustacean group
298 (Fig. 2a).

299 Assimilation efficiency (AE) for zooplankton is typically set to be a fixed fraction of
300 ingested material in models (between 0.6-0.8; Carlotti et al., 2000), and for crustacean

301 zooplankton in COBALTv2, it is set to 0.7, allowing for 70% of all food consumed to be
302 assimilated independent of prey concentration. However, for pelagic tunicates, in particular
303 appendicularians, there is evidence of AE declines as prey concentration increases, due to
304 development of tears of their pharyngeal filter and active prey rejection with increasing food
305 (Acuña and Kiefer, 2000; Lombard et al., 2009a, 2011). Retention and assimilation efficiencies
306 for salps and doliolids also vary widely, from 28-90%, which may be due to prey selectivity for
307 optimal sizes and preferred taxa (Andersen, 1986; Dadon-Pilosof et al., 2019; Pakhomov, 2004;
308 Pakhomov et al., 2006; Vargas and Madin, 2004; Walters et al., 2019). While we have
309 implemented prey selectivity in the feeding relationships, there is still evidence for feeding
310 apparatus clogging at high food concentrations due to the formation of a food bolus (Harbison et
311 al., 1986). Therefore, we implemented varying assimilation efficiencies for pelagic tunicates:

$$312 \quad AE = AE_{max} - \left((AE_{max} - AE_{min}) \left(\frac{P}{K_{AE} + P} \right) \right) \quad (\text{eq. 3})$$

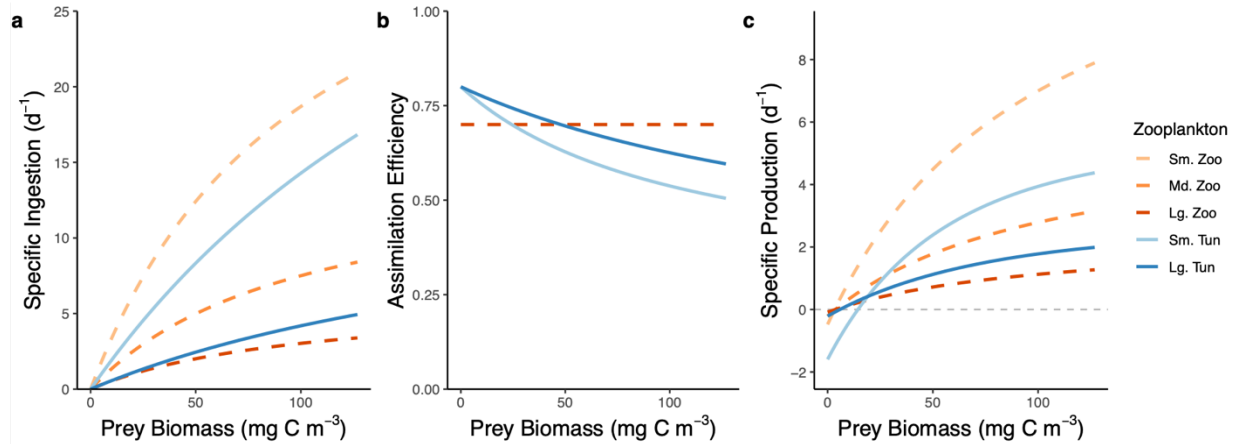
313 where AE_{max} and AE_{min} are maximum and minimum assimilation efficiencies, respectively, and
314 K_{AE} is the half-saturation constant for AE (all dimensionless).

315 This AE equation is a desaturating functional form (Hollings Type II subtracted from
316 AE_{max})(see also Berline et al., 2011). For small tunicates, AE_{max} and AE_{min} were 0.7 and 0.25,
317 respectively, and K_{AE} was 110 mg C m⁻³, which is at the low end of the range for the
318 appendicularian *O. dioica* (145.52 +/- 33.36 std. err.) as measured by Lombard et al. (2009). For
319 large tunicates, to simulate the clogging response, we also used the same AE bounds as small
320 tunicates but with a K_{AE} of 215 mg C m⁻³, a value at which approximately half of the *Pegea*
321 *confoederata* salps studied by Harbison et al. (1986) would form boluses. The difference in K_{AE}
322 between the tunicates results in the AE declining faster for small tunicates compared to their
323 larger counterparts (Fig. 2b).

324 Non-assimilated egestion losses for tunicates were parameterized similar to large
325 zooplankton with 100% of the detritus losses going towards sinking particulate organic matter
326 and no dissolved organic matter generated through grazing. This assumption is consistent with
327 the representation of small tunicates in Berline et al. (2011) and the observation that tunicate
328 detritus, representing the sinking houses of appendicularians and salp fecal pellets, are an
329 important source of zooplankton detritus (Alldredge and Silver, 1988), and contribute
330 significantly to carbon export fluxes (Alldredge, 2005; Andersen, 1998; Luo et al., 2020;
331 Robison, 2005).

332 In GZ-COBALT, we did not modify the sinking speed of GZ-mediated detritus, which is
333 pooled together with non-gelatinous detritus and sinks at a rate of 100 m d⁻¹ (Alldredge and
334 Silver, 1988; Stock et al., 2014a; Turner, 2015). While studies have shown that GZ detritus can
335 sink at rates greatly exceeding that of marine aggregates and crustacean zooplankton fecal pellets
336 (Lebrato et al., 2013), we opted to focus this study on the impact of gelatinous zooplankton,
337 specifically tunicates, within the euphotic zone and leave the assessment of GZ-mediated export
338 on biogeochemical cycles at depth to future work.

339



340
341 **Figure 2.** Specific ingestion (a), assimilation efficiency (b), and specific production (c) as a function of generalized
342 prey biomass at 25°C for zooplankton in GZ-COBALT. The three original COBALTv2 zooplankton types (small,
343 medium, and large zooplankton; dashed lines) are unchanged in all GZ-COBALT simulations from the COBALTv2
344 control model.

345
346

347 2.2.3 Metabolism and respiration

348 In the COBALTv2 base model, the total zooplankton respiration rate is a sum of the basal
349 and active respiration rate, with the former the resting metabolic rate that is proportional to
350 biomass and the latter a fixed fraction of the ingestion rate (Flynn, 2005; Stock et al., 2014a).
351 Pelagic tunicates are true filter feeders, and in contrast with crustacean zooplankton, are
352 constantly in motion regardless of the food concentration, pumping water via tail oscillations
353 (appendicularians), muscle contractions (salps), and ciliary action (doliolids and pyrosomes)
354 (Deibel, 1998; Madin and Deibel, 1998). Therefore, a truly “basal” respiration rate only occurs
355 when the tunicate is anesthetized. For *Salpa fusiformis*, swimming accounts for over half of total
356 oxygen demand (Trueman et al., 1984), while for the appendicularian *O. dioica*, swimming
357 accounted for roughly 34% of active respiration (Lombard et al., 2005). Furthermore, Lombard
358 et al. (2005) found that there was no significant difference between the respiration levels of
359 appendicularians at various food levels (no food, low, and high food), implying that the energy
360 required to digest food was small compared to the energetic requirements of swimming. In
361 contrast, the basal respiration rates for crustacean zooplankton are relatively low compared to
362 respiration rates while feeding, which increase linearly with ingestion (Kjørboe et al., 1985).
363 Thus, a key contrast that is built into GZ-COBALT is the difference between crustacean and
364 gelatinous zooplankton respiration tradeoffs: crustaceans have relatively high active respiration
365 rate (30% of ingestion) but low basal respiration, whereas GZ have low active respiration (15%
366 of ingestion) but high basal respiration rates. Consequently, compared to crustacean zooplankton,
367 tunicates incur a higher metabolic cost in low food concentrations, which prevents them from
368 accumulating biomass in large portions of the subtropical gyres. These tradeoffs can be seen on a
369 plot of specific production as a function of food concentration (Fig. 2c), and is most obvious
370 when comparing small tunicates vs. small mesozooplankton, as the tunicate specific production
371 remains negative for a greater portion of the low food concentrations. A full comparison of
372 parameters is found in Table 1.

373 Biomass-specific basal respiration for small tunicates was calculated using relationships
374 for *O. dioica* (Lombard et al., 2005). A laboratory study in the absence of food found that a 6.68
375 $\mu\text{g C}$ individual at 0°C has a weight-specific oxygen consumption of 0.068 (0.055-0.085) μmol

376 O_2 ($\mu\text{mol C}^{-1} \text{d}^{-1}$) (Lombard et al. 2005). Assuming a general zooplankton respiratory quotient of
 377 0.87 (Mayzaud et al., 2005), this translates to a basal respiration of 0.047-0.074 d^{-1} . We opted to
 378 use a value at the low end of the range (0.047 d^{-1}), so as to avoid complete elimination of their
 379 biomass in subtropical environments, where they are found in low concentrations (Steinberg et
 380 al., 2008).

381 For large tunicates, GZ-COBALT takes advantage of the mean allometric respiration
 382 relationship compiled by Luo et al. (2020) from observations in Madin and Deibel (1998; and
 383 references therein). With an average large tunicate of 1.5 mg C in that study respiring $2.5\text{E-}3$
 384 ($8.0\text{E-}4 - 8.1\text{E-}3$) $\text{mmol } O_2 \text{ mg C}^{-1} \text{d}^{-1}$, and using a salp-specific respiratory quotient of 1.16
 385 (Mayzaud et al., 2005), basal respiration varied by an order of magnitude (0.011-0.11 d^{-1}) with
 386 mean of 0.035 d^{-1} . However, even with this large uncertainty range, Luo et al. (2020) found that
 387 under average conditions in the pelagic oceans, even the lower bound of these respiration rates
 388 were too high, such that metabolic demands exceeded available food resources, yielding
 389 unfavorable conditions for survival, particularly in the subtropical gyres. Therefore, in the
 390 baseline model configuration, we used a basal respiration rate (0.008 d^{-1}) that was slightly below
 391 the lower bound, tuned to ensure realistic gelatinous zooplankton in oligotrophic ecosystems.
 392 This choice is consistent with the strategy enlisted for calibrating the basal metabolic costs of the
 393 crustacean zooplankton (Stock and Dunne, 2010) wherein highly uncertain basal metabolic rates
 394 were calibrated to ensure that the simulated biomass was consistent with observations in the
 395 oligotrophic gyres where the impact of basal metabolic costs are most prominent. In nature, To
 396 explore the effect of this tuning, a sensitivity case was run where large tunicate basal respiration
 397 was set to the mean value from allometry (Section 2.3).

398 399 2.2.4 Other sources of mortality

400 Another key difference between the small and large tunicates is in the additional sources
 401 of mortality. While small tunicates primarily experience mortality through predation, large
 402 tunicates experience cold temperature reproductive failures (Henschke and Pakhomov, 2019) as
 403 well as mass mortality events (jelly-falls) (Henschke et al., 2015; Lebrato and Jones, 2009).
 404 Large tunicate aggregation losses, representing jelly-falls, were parameterized as a quadratic loss
 405 that is suppressed when food is plentiful, following the same functional form as the
 406 phytoplankton aggregation losses as a function of nutrient limitation in COBALTv2 (Stock et al.,
 407 2020; Waite et al., 1992) and other global biogeochemical models (e.g., PISCES; Aumont et al.,
 408 2015). The aggregation losses are controlled by two parameters: f_{agg} , which represents the
 409 fraction of the maximum ingestion rate above which aggregation losses are suppressed, and m_{agg} ,
 410 or a maximum aggregation loss rate. f_{agg} was set to 0.1 to account for the salp ability to tolerate
 411 low food concentrations, and m_{agg} was set to $1.0\text{E-}3 \text{ m}^3 \text{ mg C}^{-1} \text{d}^{-1}$ to achieve jelly-falls
 412 representing approximately 35% of total large tunicate mortality following Luo et al. (2020).

413
414
415 **Table 1.** GZ-COBALT zooplankton ingestion, respiration, and aggregation parameters. Plankton functional types
 416 (PFT)s: smt = small tunicates, lgt = large tunicates, smz = small zooplankton, mdz = medium zooplankton, and lgz =
 417 large zooplankton.

Parameter	Name (Units)	PFT	Values	References
I_{max}	Maximum ingestion rate (day^{-1})	smt	1.875	(Lombard et al., 2009a)
		lgt	0.55	(Luo et al., 2020; Madin and Deibel, 1998)
		smz	1.42	

		mdz	0.57	(Hansen et al., 1997; Stock et al., 2020; Stock and Dunne, 2010)
		lgz	0.23	
K_i	Ingestion half-saturation constant (mg C m^{-3})	smt, lgt	250	(Acuña and Kiefer, 2000; Gibson and Paffenhöfer, 2000)
		smz, mdz, lgz	102	(Stock et al., 2014a, 2020)
b_{resp}	Basal respiration rate (day^{-1})	smt	0.06	(Lombard et al., 2005)
		lgt	0.008	(Luo et al., 2020; Madin and Deibel, 1998); tuned to allow for sufficient biomass in subtropical gyres
		smz	0.018	(Hansen et al., 1997; Stock et al., 2020; Stock and Dunne, 2010)
		mdz	0.008	
		lgz	0.0032	
f_{aresp}	Fraction of ingestion rate for active respiration (dimensionless)	smt, lgt	0.15	See text; also tuned to allow for sufficient biomass in subtropical gyres
		smz, mdz, lgz	0.3	(Stock et al., 2014a, 2020)
AE_{min}, AE_{max}	Minimum and maximum assimilation efficiency (dimensionless)	smt, lgt	0.25, 0.8	(Lombard et al., 2009a; Madin and Deibel, 1998; Pakhomov et al., 2006)
		smz, mdz, lgz	0.7, 0.7	(Stock et al., 2014a, 2020)
K_{AE}	Assimilation efficiency half-saturation constant (mg C m^{-3})	smt	110	(Berline et al., 2011; Lombard et al., 2009a)
		lgt	215	(Harbison et al., 1986)
		smz, mdz, lgz	N/A	N/A
f_{agg}	Fraction of maximum ingestion at which aggregation mortality is suppressed (dimensionless)	lgt	0.1	See text
m_{agg}	Maximum aggregation loss rate ($\text{m}^3 \text{ mg C}^{-1} \text{ d}^{-1}$)	lgt	1.0E-3	Calibrated to achieve jelly-falls representing 35% of total mortality

418
419
420
421

2.4 Physical Framework

422 The GZ-COBALT model with 35 tracers was run in a global ocean-ice configuration
423 using the GFDL models Modular Ocean Model 6 (MOM6) and Sea Ice Simulator 2 (SIS2) in a
424 nominal 0.5° , or roughly 50 km, horizontal resolution (OM4p5, Adcroft et al., 2019). The 0.5°
425 horizontal grid improves the resolution of boundary currents compared to earlier generations of
426 1° MOM models. The vertical coordinate in MOM6 is a hybrid z^* -isopycnal vertical coordinate
427 system implemented using an Arbitrary Lagrangian-Eulerian (ALE) method, such that isopycnal
428 coordinates are used in the ocean interior and a z^* coordinate is used in the mixed layer. OM4p5
429 uses 75 vertical layers, which allows for finer resolution at the ocean surface (~ 2 m) compared to
430 earlier model configurations with 10 m surface resolution and 50 vertical layers (Adcroft et al.,
431 2019). The ocean and ice model configurations are also equivalent to those components used
432 within the fully-coupled ESM4.1 model (Dunne et al., 2020).

433 Model simulations were forced using Common Ocean-Ice Reference Experiment II
434 (CORE-II) (Large and Yeager, 2009), a 60-year interannually varying dataset representing
435 atmospheric forcings from 1948-2007. The model was initialized similar to that of the fully-
436 coupled model (Stock et al., 2020): from World Ocean Atlas 2013 (WOA13) data for
437 temperature, salinity, oxygen, and dissolved inorganic nutrients (Garcia et al., 2013a, 2013b;
438 Locarnini et al., 2013; Zweng et al., 2013), and from Global Ocean Data Analysis Project
439 (GLODAPv2) for dissolved inorganic carbon and alkalinity (Lauvset et al., 2016). Other tracers
440 were initialized from outputs of a previous version of COBALT (Stock et al., 2014a), and the
441 two new gelatinous zooplankton tracers were initialized with biomass concentrations similar to
442 medium and large zooplankton. Additional sources of nutrients include atmospheric deposition
443 of NH_4 and NO_3 (Horowitz et al., 2003), dust from Zhao et al. (2018) with soluble Fe calculated
444 in accordance with Baker and Croot (2010), as well as coastal iron and river nutrients from the
445 GlobalNEWS dataset (Seitzinger et al., 2005), as described in (Stock et al., 2020)

446 GZ-COBALT was run for one 60-year interannual forcing cycle. Results are reported
447 from a climatology computed from the last 20 years of model simulation, representing 1988-
448 2007. A COBALTv2 control simulation with the same exact model setup, but with tunicates
449 turned off, was also run for 60 years.

450

451 2.5 Parameter Sensitivity Runs

452

453 To understand the impact of the unique aspects of GZ physiology and ecology as
454 described above on their emergent distribution and productivity, we considered a number of
455 perturbations around the baseline settings described above. These sensitivity runs (Table 2)
456 examine both the effect of our tuning choices (cases 1-2) as well as some key tradeoffs relative
457 to crustacean zooplankton (cases 3-5). All parameter sensitivity runs were conducted following
458 the same physical forcing as the GZ-COBALT base simulation.

459

- 460 1) For large tunicates, the basal respiration rate was adjusted to be slightly below the
461 lower bound from the literature. Sensitivity case 1 examines the effects of using the
462 mean basal respiration rate from allometric relationships from the literature.
- 463 2) For the baseline GZ-COBALT model, we used a maximum ingestion rate of small
464 tunicates at the lower bound of the range. For sensitivity case 2, we test a case where
465 the small tunicates' I_{max} is higher, set to the mean of the literature-based range.
- 466 3) Sensitivity case 3 explores the impact of the unique feeding behavior of GZ relative
467 to crustaceans. For the calibrated model (base case), we used a mean K_i value from a
468 wide range measured by Acuña and Kiefer (2000). However, models are known to be
469 quite sensitive to this relatively unconstrained parameter (Stock and Dunne, 2010).
470 Thus, we ran a sensitivity test where the tunicate K_i values were the same as that of
471 the crustacean zooplankton. Since the maximum ingestion rate (I_{max}) was set in
472 combination with the K_i values to achieve specific filtration rates at low prey
473 concentrations consistent with observations, I_{max} was also modified accordingly to
474 preserve the observational constraint.
- 475 4) Sensitivity case 4 examines another unique aspect of pelagic tunicates feeding
476 relative to that of crustaceans. In the baseline GZ-COBALT, we implemented varying
477 assimilation efficiency (AE) following Berline et al. (2011). To explore the
478 uncertainty associated with this assumption, we ran a sensitivity test where the

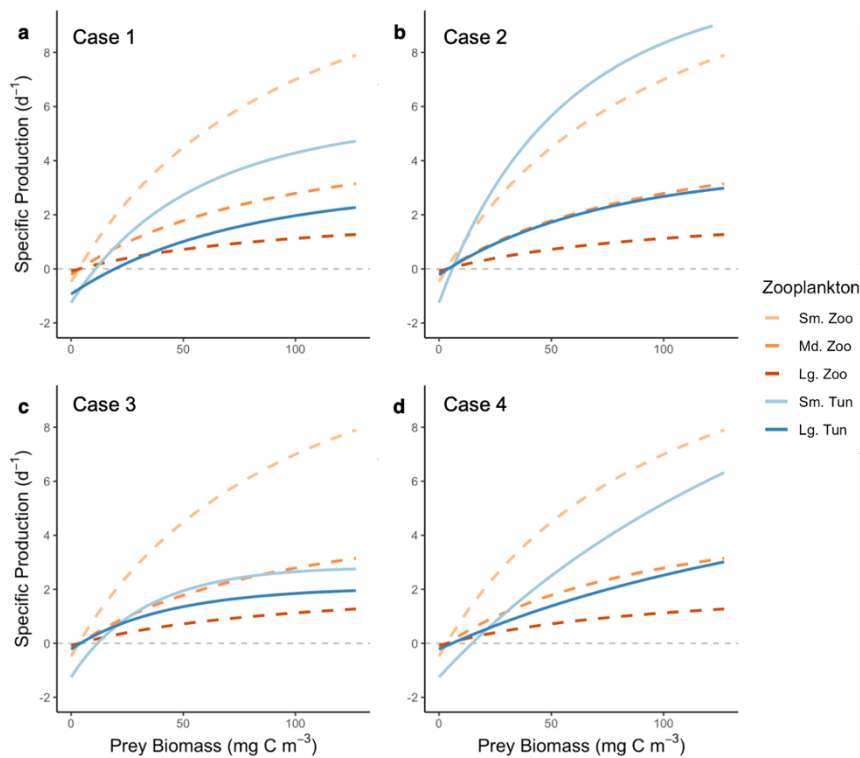
479 tunicates' AE were constant, but set at a slightly lower value than other zooplankton,
 480 to account for their comparatively lower retention rates.
 481 5) Finally, a case was run to explore the impacts of ignoring the role of large tunicate
 482 aggregation mortality (representing jelly-falls).
 483

484 To illustrate the impact of these various parameter modifications, we computed the
 485 specific production of all zooplankton groups under an idealized condition of 25°C with a
 486 generalized prey biomass (Fig 3), which can be contrasted against the GZ-COBALT baseline
 487 (Fig. 2c).
 488

489 **Table 2.** Parameters tested in sensitivity tests, showing the values in the base code as well as the permutation for the
 490 individual sensitivity case. For detailed names of parameters, see Table 1. Plankton functional types (PFTs): smt =
 491 small tunicates; lgt = large tunicates.

Case #	Parameter	PFT	Base code	Permutation
1	b_{resp} (d^{-1})	lgt	0.008	0.035
2	I_{max} (d^{-1})	smt	1.875	3.25
3	I_{max} (d^{-1}), K_i ($mg\ C\ m^{-3}$)	smt	1.875, 250	0.765, 102
		lgt	0.55, 250	0.22, 102
4	AE_{min} , AE_{max}	smt & lgt	0.25, 0.8	0.6, 0.6
5	m_{agg} ($m^3\ mg\ C^{-1}\ d^{-1}$)	lgt	1.0E-3	0

492
 493



494 **Figure 3.** Specific production as a function of generalized prey biomass at 25°C for sensitivity cases 1-4 (a-d). The
 495 three original COBALTv2 zooplankton types (small, medium, and large zooplankton; dashed lines) are unchanged
 496

497 in all GZ-COBALT simulations from the COBALTv2 control. The specific production in sensitivity case 5 is the
498 same as the base case (Fig. 2c).

499
500

501 **2.6 Validation data**

502

503 As described in the introduction, a central question in our analysis is whether the model can
504 simultaneously reconcile recent measurements suggesting that GZ carbon biomass is *ca.* 10x
505 greater than previously thought while also satisfying core observational constraints on crustacean
506 biomass, nutrients, chlorophyll and net primary production (NPP). The subsections that follow
507 describe the datasets compiled and/or enlisted for each of these tasks, and the analyses used to
508 assess model-data consistency across trophic gradients and ocean biomes.

509

510 *2.6.1 Pelagic tunicate dataset and model-data comparison*

511 To generate biomass validation data for pelagic tunicates, we updated the gridded
512 tunicate data (primarily salps) from Luo et al. (2020) with additional data on both thaliaceans and
513 appendicularians from the NOAA Coastal and Oceanic Plankton Ecology, Production, and
514 Observation Database (COPEPOD) (O'Brien, 2014). From the COPEPOD database, raw data on
515 urochordates were extracted and divided into small tunicates (all appendicularians) and large
516 tunicates (salps, doliolids, and pyrosomes). With the exception of data from the ECOSAR-II
517 cruise (Muxagata, 1999), all other data were in numeric density only (# individuals m⁻³).
518 Numeric density data were first converted to a common 330 µm mesh size (Moriarty and
519 O'Brien, 2013; O'Brien, 2005). Second, since the geometric mean cannot handle zeros, zero
520 numeric density values were modified to be a non-zero value slightly below the minimum value
521 for both size fractions (small: 0.0008 ind. m⁻³, large: 0.001 ind. m⁻³). Next, numeric density was
522 converted to carbon biomass using the characteristic individual biomass values defined in section
523 2.2.3 (appendicularians: 6.7 µg C, salps: 1.5 mg C). Characteristic biomass values for pyrosomes
524 and doliolids were 22.9 mg C ind⁻¹ (100 mm individual) and 19.2 µg C ind⁻¹ (5 mm individual),
525 respectively, following Lucas et al. (2014), which used regression conversions from Gibson and
526 Paffenhöfer (2000) and Mayzaud et al. (2007). Using the geometric mean, 1° gridded values
527 were averaged by month, then year, for an annual mean biomass. Finally, the Jellyfish Database
528 Initiative (JeDI; Condon et al., 2015) database was additionally queried for appendicularian data.
529 Data from 90 additional 1° grid cells, primarily from the North Atlantic and Eastern Equatorial
530 Pacific, were present in the JeDI dataset but not in the COPEPOD database. These data were
531 added to our validation dataset. Appendicularian data were present in a total of 3,914 1° grid
532 cells (Fig. 4a).

533 Thaliacean data from the COPEPOD database were combined with the Luo et al. (2020)
534 gridded salp data, which primarily included gridded biomass data from Lucas et al. (2014), with
535 updates from JeDI the Palmer LTER site at the Western Antarctic Peninsula (Steinberg et al.,
536 2015), and KRILLBASE (Atkinson et al., 2017). Out of the 5,468 grid cells with data, there were
537 1,481 cells where COPEPOD data were only present, 1,952 cells where the Luo et al. (2020) data
538 were only present, and overlap at 2,035 grid cells (Fig. 4b). Because the raw data with assumed
539 lengths and carbon conversions from Lucas et al. (2014) were not available, we were unable to
540 examine individual data points for overlap and cross-validation. However, a broad examination
541 of the two datasets revealed that at the areas of overlap, carbon biomass compiled from
542 COPEPOD was 1.4x (geometric mean) that of Luo et al. (2020), with variations likely due to the
543 finer taxonomic detail of the Lucas et al. (2014) effort. This was within the uncertainty bounds

544 that we considered acceptable (roughly 2x uncertainty). Ultimately, due to discrepancies in
545 classification and specificity over time (e.g., broad categories such as “Tunicata” and “Salps and
546 doliolids” were dominant in classifications from the 1950’s and 1960’s, but not later), we
547 decided that using a single characteristic carbon biomass conversion for each broad taxonomic
548 category in the COPEPOD data gave a taxonomic specificity consistent with the coarsest
549 taxonomic specificity in the data. Further, this single biomass conversion removed a persistent
550 discontinuity in the Luo et al. (2020) carbon biomass values in the Indian Ocean south of 5°N
551 that we were previously unable to resolve. Since the vast majority of the JeDI data sources in the
552 Indian Ocean were from the 1959-1965 International Indian Ocean Expedition (IIOE), which are
553 also present in COPEPOD (Condon et al., 2015), we opted to replace the Luo et al. (2020) Indian
554 Ocean data with the COPEPOD data during our merge. For the rest of the oceans, we merged the
555 two datasets by taking the geometric mean at every grid cell where there was overlap.

556 Ultimately, the discrepancies between the datasets were quite low compared to the
557 differences in biomass due to sampling type, particularly when comparing extractive (nets) vs.
558 non-extractive (imaging) methods. Since traditional, net-based sampling systems break apart
559 fragile organisms such as pelagic tunicates and other gelatinous zooplankton, a biomass
560 adjustment is necessary to account for the reduced sampling from nets. Remsen et al. (2004)
561 used concurrent sampling with an imaging system and a 162 µm mesh plankton net, and found
562 that for pelagic tunicates, their abundance was undersampled by nets by a factor of 3-4x, and
563 their carbon biomass undersampled by a factor of 5-15x. Therefore, we considered an additional
564 “adjusted biomass” from samples with a 10x increase relative to the unadjusted biomass. We
565 focus mainly on this adjusted biomass, which is indicative of nascent appreciation of the likely
566 broader importance of gelatinous zooplankton as revealed by optical instruments. This is also
567 consistent with our intent to assess whether these high values can be reconciled with the overall
568 high abundance of mesozooplankton in many regions.

569 We complement our assessment of the simulated magnitude of tunicate biomass with one
570 of the relationship between tunicate biomass and other ecosystem properties spanning
571 oceanographic gradients. As the spatial gradients in tunicate biomass span 5 orders of magnitude,
572 this assessment provides a second metric less sensitive to the adjustments above. To do this, we
573 considered the GZ biomass as a function of chlorophyll concentration. The resultant, large-scale
574 relationship allowed for contrasts between large and small tunicates, and between tunicates and
575 crustaceans. For chlorophyll, we used the GlobColour merged satellite chlorophyll product (from
576 MERIS, MODIS-Aqua, and SeaWiFS) monthly climatology for case 1 waters using the weighted
577 averaging method, blended at latitudes south of 50°S with the Southern Ocean algorithm of
578 Johnson et al. (2013). We computed a growing season mean, define as all months for latitudes
579 between 30°N and 30°S, and spring and summer only for latitudes poleward of 30°N/S. The
580 slope of the log-log relationships between chlorophyll and the biomass of small tunicates, large
581 tunicates, and crustacean mesozooplankton (Moriarty and O’Brien, 2013; more details in Section
582 2.6.3) were established as emergent relationships for validation purposes.

583 584 2.6.2 Biome definitions

585 Finally, we assess gelatinous zooplankton simulation as a function of ocean biome,
586 adjusting for any systematic biases in the model by referencing biome locations to chlorophyll,
587 light, and temperature thresholds. We used the three major ocean biomes of Stock et al. (2014),
588 following Banse (1992): 1) Low Chlorophyll (LC), which encompasses the subtropical gyres, 2)
589 High Chlorophyll Seasonally Stratified (HCSS), which encompasses the high latitudes, and 3)

590 High Chlorophyll Permanently Stratified (HCPS), which includes the coastal and equatorial
591 upwelling regions. Stock et al. (2014) used a threshold of $0.125 \text{ mg Chl m}^{-3}$ to separate between
592 the low vs. high chlorophyll regions in observational chlorophyll datasets. In our biome
593 definition, we first calculated the total ocean area with observational chlorophyll values lower
594 than that threshold (approximately 40% of the world's oceans), then found the model chlorophyll
595 threshold that resulted in a model LC area that most closely matched the LC surface area from
596 observations. For the COBALTv2 control and GZ-COBALT, this threshold was 0.162 and 0.184
597 mg Chl m^{-3} , respectively. Next, to distinguish between the seasonally vs. permanently stratified
598 regions, we used the minimum of the mixed layer irradiance climatology (light averaged over the
599 mixed layer). HCSS regions were demarcated as those with minimum mixed layer irradiances
600 lower than 5 W m^{-2} , while the opposite was true of HCPS. Using mixed layer irradiance more
601 accurately defined the seasonal seas vs. upwelling areas, preventing HCPS areas from occurring
602 in Arctic regions with shallow maximum mixed layers (Stock et al., 2014a). Biomes for both
603 GZ-COBALT and the COBALTv2 control are shown in Fig. S1.

604

605 *2.6.3: Crustacean zooplankton dataset and model-data comparison*

606 To assess whether pelagic tunicate biomass magnitude and cross-biome gradients can be
607 represented while maintaining crustacean zooplankton populations consistent with observations,
608 we used the 2012 gridded carbon biomass data compilation from the COPEPOD database
609 (Moriarty and O'Brien, 2013). The entire COPEPOD database (O'Brien, 2014) consists of
610 multiple types of data products, including the raw, taxonomic data as used above for pelagic
611 tunicates, as well as the Moriarty and O'Brien (2013) carbon biomass compilation, which is the
612 more commonly used dataset for mesozooplankton model validation. In total, the COPEPOD
613 global carbon biomass compilation includes over 150,000 data points that were converted to an
614 equivalent $333 \mu\text{m}$ mesh net size, with each gridded value representing multiple data points.
615 Given the net-based sampling and the historical focus on crustacean zooplankton, the vast
616 majority of the individual data points consisted of hard-bodied mesozooplankton. Thus, we used
617 the COPEPOD global carbon biomass compilation as a proxy of crustacean mesozooplankton to
618 compare against the small and large crustacean mesozooplankton in GZ-COBALT.

619 Similar to the GZ data, the crustacean observations were also scaled with chlorophyll on
620 a log-log scale. This enabled us to make comparisons along trophic gradients and across biomes
621 for crustaceans and gelatinous zooplankton.

622 Finally, in addition to GZ and crustacean constraints, we include a suite of standard
623 biogeochemical metrics to ensure that the model solution satisfies large-scale productivity and
624 nutrient patterns. The data we used were the dissolved inorganic nutrient concentrations (NO_3 ,
625 PO_4 , and SiO_3) at the ocean surface from the World Ocean Atlas (WOA) 2018 (Garcia et al.,
626 2019).

627

628

629 3. Results

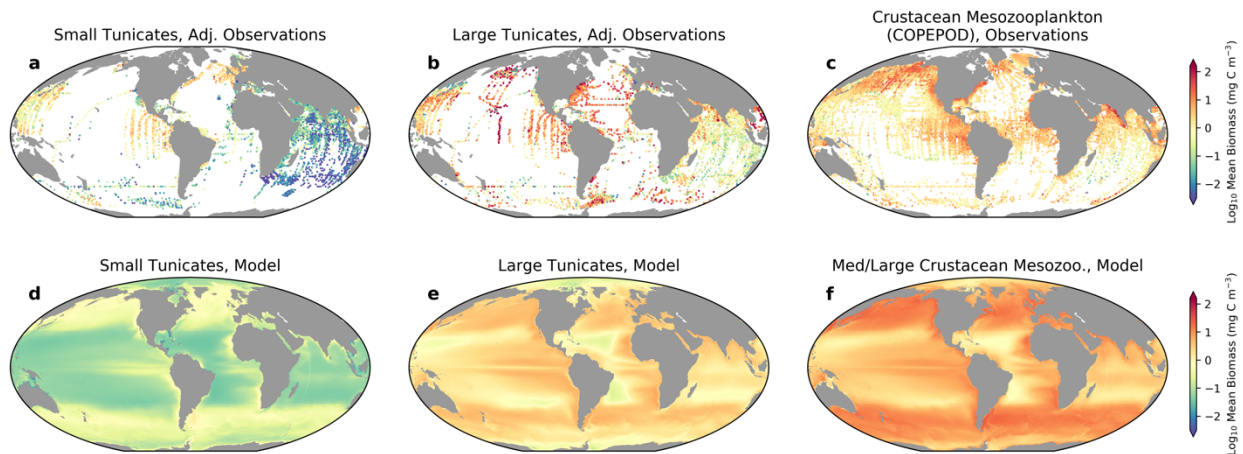
630

631 3.1 Global distribution and biomass-chlorophyll scaling

632 The GZ-COBALT simulation produced values consistent with the adjusted biomass of
633 small and large pelagic tunicates, while also reproducing observed crustacean biomass and
634 satisfying ocean biogeochemical constraints (Figs. 4-5, Tables 3-4). Global NPP was 53.7 Pg C
635 y^{-1} and export flux at 100 m was 6.36 Pg C y^{-1} in GZ-COBALT, compared to 55.4 and 6.23 Pg C
636 y^{-1} in COBALTv2. Surface chlorophyll and macronutrient concentrations in GZ-COBALT also
637 compared well with the COBALTv2 control and observational constraints (Fig. 5).

638 The modeled global mean annual biomass integrated over the top 100 m was 5.8 Tg C for
639 small tunicates and 81.5 Tg C for large tunicates, yielding a total 100 m biomass of 87 Tg C. A
640 small but non-negligible fraction of tunicate biomass was below 100 m, even with the model
641 lacking vertical migration, such that the water column integrated biomass was 102 Tg C. These
642 values are within the adjusted mean and uncertainty of the observations. In comparison, the
643 medium/large crustacean mesozooplankton biomass (representing the size fraction most closely
644 comparable to the values in COPEPOD database) in GZ-COBALT was 205 Tg C in the top 100
645 m, which was slightly lower than the COBALTv2 value of 220 Tg C. Observational estimates of
646 large mesozooplankton biomass from COPEPOD, using a biome-specific geometric mean and
647 standard deviation to extrapolate globally, was 133 (+/- 209) Tg C over the top 200 m. See Table
648 3 for additional comparisons by major ocean biome.

649



650

651 **Figure 4.** Global mean distributions of small and large tunicates and crustacean mesozooplankton, comparing
652 tunicate adjusted observations (a,b), large crustacean biomass from COPEPOD (c) with results from the top 100 m
653 of the model (d,e,f). Medium/large crustacean mesozooplankton model values are given as the large
654 mesozooplankton plus 0.5*small mesozooplankton. Model data show the time-average of the growing season only
655 (fall and winter months excluded poleward of 30°N/S).

656

657

658

659

660

661

662

663

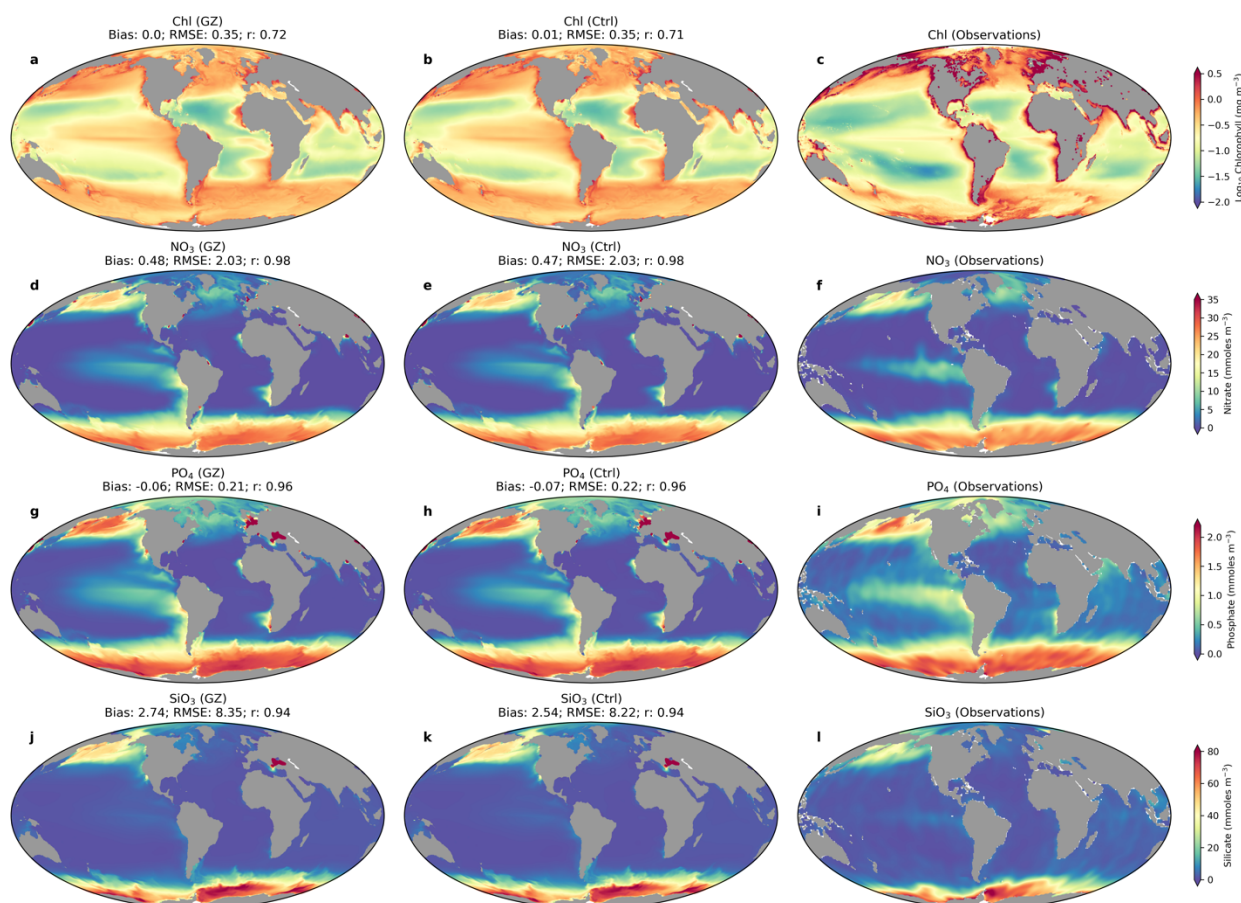
664

665

666 **Table 3.** Global and biome-specific biomass comparison of the observations and the GZ-COBALT model. Model
 667 results are the annual area weighted mean of the top 100 m carbon biomass. Observational values are given as the
 668 geometric mean and geometric standard deviation of values within the biomes, with global geometric standard
 669 deviation calculated following the procedure in Luo et al. (2020). Biomes: LC = Low Chlorophyll; HCPS = High
 670 Chlorophyll Permanently Stratified; HCSS = High Chlorophyll Seasonally Stratified. See Fig. S1 for biome maps.

Biome	Large Tunicates (mg C m ⁻³)		Small Tunicates (mg C m ⁻³)		Med/Large Crustacean mesozooplankton (mg C m ⁻³)	
	Adj. Obs. mean (stdev)	Model annual mean	Adj. Obs. mean (stdev)	Model annual mean	Obs. mean (stdev)	Model annual mean
LC	1.4 (10)	1.4	0.05 (16)	0.06	0.98 (2.3)	2.6
HCPS	1.9 (8.0)	3.2	0.11 (15)	0.16	3.6 (2.5)	6.6
HCSS	2.9 (11)	2.4	0.08 (23)	0.28	2.9 (3.2)	8.3
Global	2.0 (9.9)	1.6	0.07 (18)	0.11	2.0 (3.1)	4.1

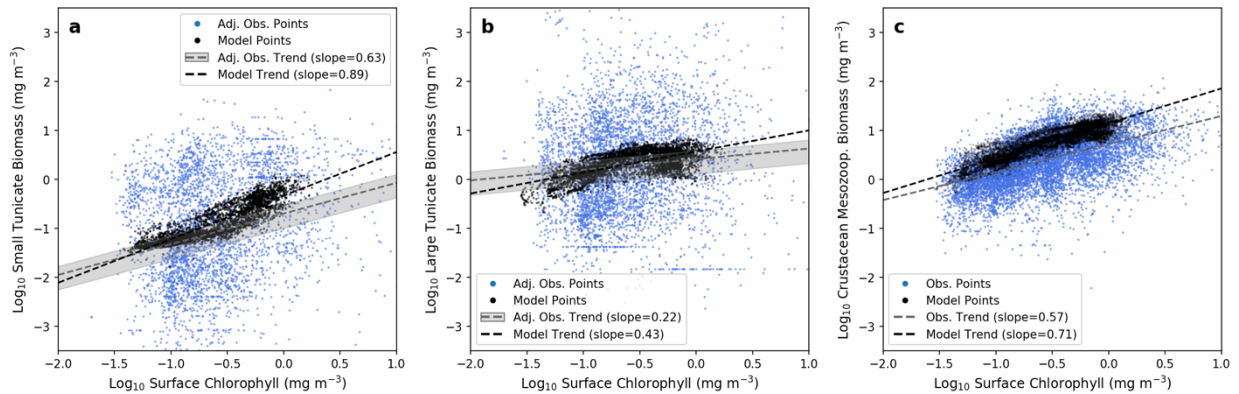
671
672



673 **Figure 5.** Surface chlorophyll, log₁₀ scale (mg Chl m⁻³, a-c) and nutrients (mmol NO₃ m⁻³, d-f; mmol PO₄ m⁻³, g-i;
 674 mmol SiO₃ m⁻³, j-i) from GZ-COBALT (left column; a, d, g, j), the COBALTv2 Control (center column; b, e, h, k),
 675 and observations (right column; c, f, i, l). Model bias, root mean squared error (RMSE), and Pearson's correlation
 676 coefficient (r) are also reported.
 677
 678

679 In the observations, we found that there was a contrast in the slope and intercept of
 680 biomass-chlorophyll scaling relationship between small tunicates, large tunicates, and crustacean
 681 mesozooplankton (Fig. 6). The small tunicates had significantly less biomass and a steeper log-

682 log slope (0.63 +/- 0.045 residual std. err.; Fig. 6a) than the large tunicates, which was much
683 flatter (0.22 +/- 0.036; Fig. 6b). The crustacean mesozooplankton data had much less variability,
684 a mean biomass similar to that of the large tunicates, and a biomass-chlorophyll scaling slope a
685 little shallower than the small tunicates (slope: 0.57 +/- 0.009; Fig. 6c). GZ-COBALT
686 successfully captured the differences in mean biomass across all three groups, as well as the
687 contrast in slope between the three groups, though admittedly the modeled slopes were all
688 slightly steeper than the observational slopes. The large tunicates had the shallowest biomass-
689 chlorophyll scaling slope (0.43, Fig. 6b), followed by the crustacean mesozooplankton (0.71,
690 Fig. 6c) and the small tunicates (0.89, Fig. 6a).
691



692
693 **Figure 6.** Log-log relationship between tunicate biomass and surface chlorophyll from adjusted observations
694 (blue) and model data (black), sampled at the same locations as the observational dataset, for (a) small
695 tunicates, (b) large tunicates, and (c) crustacean mesozooplankton. The observations were adjusted from the
696 data compilation to account for the systematic low sampling bias from nets (10-fold adjustment), with the grey
697 bars around the observational regression line showing the 5-15x adjustment range. Model values are from the
698 top 100-m, and the crustacean mesozooplankton biomass was computed as large mesozooplankton + 0.5*small
699 mesozooplankton. Observational surface chlorophyll, as well as model data, were time means from the
700 growing season.

701
702 The sensitivity tests illustrated the impact of various aspects of the base GZ-COBALT
703 parameter choices, as well as the distinct physiology of tunicates relative to crustacean
704 mesozooplankton. For large tunicates, the reduced basal respiration rate, relative to the literature-
705 based mean, in the base GZ-COBALT simulation was key for achieving a mean biomass
706 consistent with observations (see case 1, Fig. S2a-c). Similarly, for small tunicates, the lower
707 maximum ingestion rate relative to the literature-based values, was also essential for achieving a
708 mean biomass consistent with observations, and a biomass-chlorophyll scaling slope that did not
709 deviate too far from the observational constraints (case 2, Fig. S2d-f). In case 2, total tunicate
710 production also doubled, despite modest increases in biomass, largely due to the role of the small
711 tunicates (Table 4). The tunicate biomass-chlorophyll scaling slope was a result of many factors,
712 including competition between tunicate size classes, as the relative increase in small tunicate
713 biomass resulted in a shallower scaling slope for large tunicates (case 2, Fig. S2e).

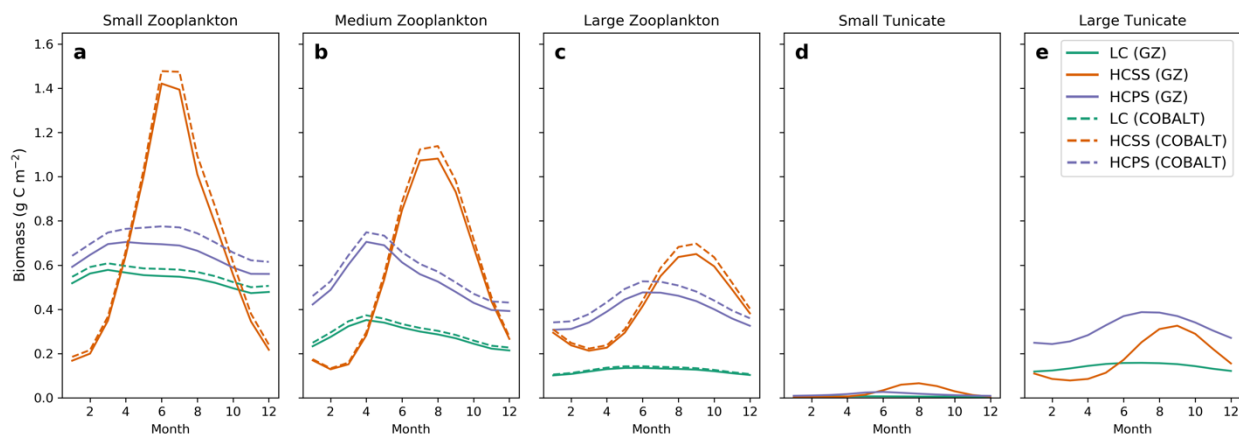
714 Sensitivity cases 3-5 focused on model formulations distinct to pelagic tunicates relative
715 to the original crustacean mesozooplankton in COBALTv2. In case 3, where the ingestion half-
716 saturation constant (with associated adjustments to the maximum ingestion rate) was set to the
717 same value as that of the crustaceans, the resultant mean biomass and biomass-chlorophyll
718 scaling for both tunicates matched the observations more closely (Fig. S2g-i). This was an
719 interesting result and could have been a tuning choice; however, doing so would have negated a

720 key criterion (of the half-saturation constant, K_i , being much greater than the prey concentration)
721 in converting measurements of clearance rate to ingestion rate. Setting the assimilation efficiency
722 to a constant value (case 4) resulted in small tunicates being closer to observations, but large
723 tunicates dropping significantly in biomass, particularly in the low productivity areas (Fig. S2j-l).
724 This suggests that the variable assimilation efficiency was one factor in allowing large tunicates
725 to survive in the subtropical gyres. Finally, in the case where large tunicate aggregation mortality
726 was removed, this resulted in large tunicate biomass greatly increasing in the high chlorophyll
727 areas, with associated increases in the biomass scaling slope (Fig. S2m-o).

728 729 3.2 Seasonal cycle

730 All zooplankton exhibited a stronger seasonal cycle in the high chlorophyll seasonally
731 stratified (HCSS) biome compared to the high chlorophyll permanently stratified (HCPS) and
732 low chlorophyll (LC) biomes, with the biomass peak shifting later in the summer as zooplankton
733 size increases. GZ exhibited a late summer (August-September) peak for both small and large
734 tunicates. The large tunicates were also unique amongst zooplankton in that their biomass in the
735 HCSS biome did not exceed that of the HCPS biome (Fig. 7). Results from the sensitivity cases
736 showed that this is largely due to the large tunicate aggregation mortality, or jelly-falls (case 5,
737 Fig. S3k-o), which serves to strongly dampen blooms. Additionally, reductions in the ingestion
738 half-saturation constant (and associated maximum ingestion rate; case 3, Fig. S3a-e) and the
739 constant assimilation efficiency (case 4) also reduced the magnitude of the blooms. Additionally,
740 in case 4, the small tunicates' bloom timing was also shifted to be slightly earlier (Fig. S3f-j). In
741 the base GZ-COBALT configuration, the biomass of the non-GZ zooplankton were overall
742 reduced compared to the COBALTv2 control (-7%, -6%, and -7.2% for small, medium, and
743 large zooplankton, respectively), with the biggest difference seen in the summer
744 microzooplankton biomass in the HCPS biome. Other substantial differences included the
745 wintertime biomass of small crustacean mesozooplankton in the LC biome, due to the low
746 starting biomass in the control (Fig. 7).

747



748
749 **Figure 7.** Seasonal cycle of modeled (a) microzooplankton, (b) medium zooplankton, (c) large zooplankton,
750 (d) small tunicates, and (e) large tunicates, separated by biome. Biome definitions: LC = low chlorophyll,
751 HCSS = high chlorophyll seasonally stratified, HCPS = high chlorophyll permanently stratified. Southern
752 Hemisphere values were shifted six months such that Austral summer is represented by months 6-8. Solid lines
753 indicate the GZ-COBALT simulation, and dashed lines show zooplankton values from the COBALTv2 control
754 simulation.

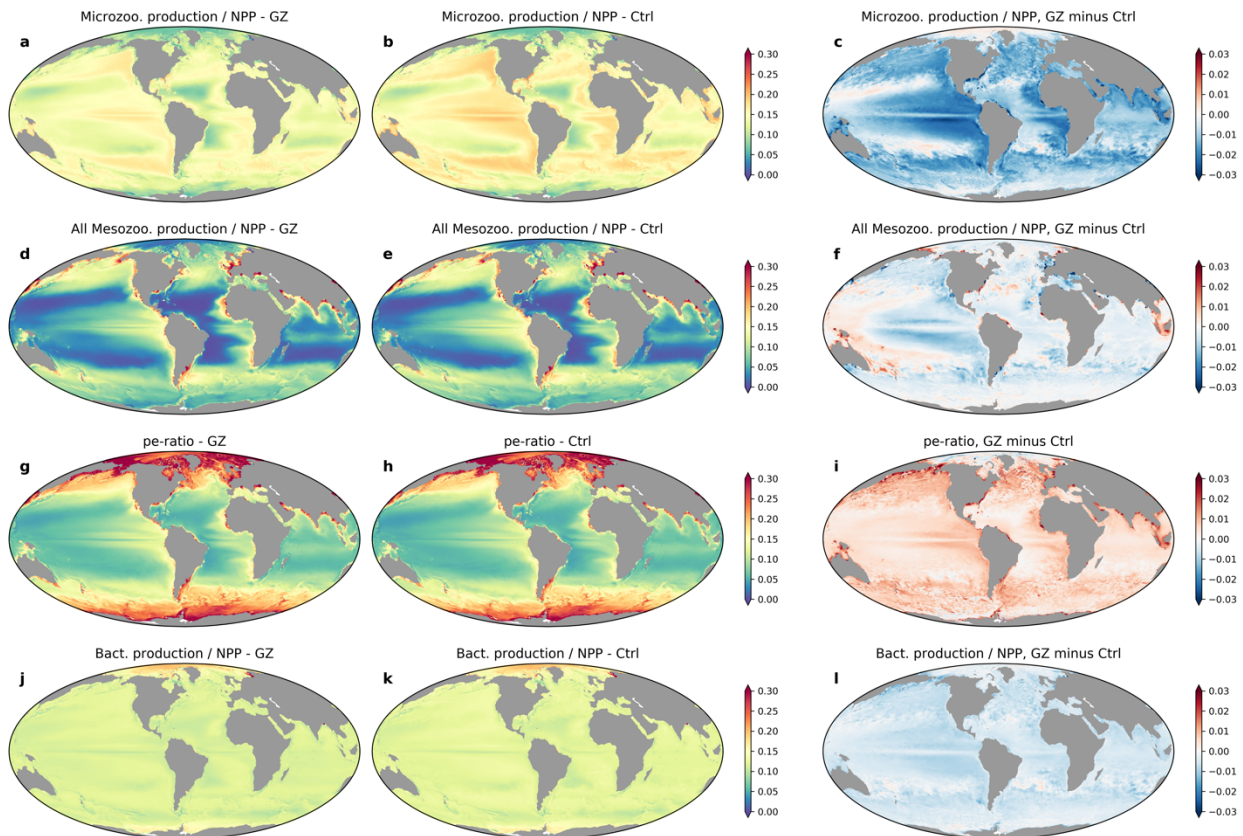
755

756 3.3. Biogeochemical impacts

757 The overall impact of gelatinous zooplankton on the partitioning of energy between the
758 microbial food web, export to depth, and energy available to higher trophic levels through
759 mesozooplankton was assessed via the difference between GZ-COBALT and the control
760 formulation (Fig. 8). This comparison suggests that the two tunicate classes have a competitive
761 interaction with microzooplankton (Fig. 8c) and a small, but net negative impact of the total
762 combined production of mesozooplankton (i.e., GZ and crustaceans, Fig. 8f). This is in spite of a
763 competitive impact on crustacean zooplankton, which was greater for the small crustaceans,
764 particularly in the upwelling zones, compared to the large crustaceans (Fig. S4).

765 The differences between the simulations becomes more pronounced when considering
766 plankton functional types that dominate recycling vs. export processes. With the addition of
767 pelagic tunicates, the routing of carbon to the microbial food-web decreased, as indicated by
768 declines in both the heterotrophic bacteria production ratio and the microzooplankton production
769 ratio (Fig. 8c, 7l). Meanwhile, the particle export ratio (pe-ratio, defined as the export flux at 100
770 m divided by NPP) increased globally (Fig. 8i). This comes as small and large tunicates
771 contributed 0.19 and 0.79 Pg C y⁻¹, respectively, of total export production in the top 100 m (of
772 which 72% sinks past 100 m). This increase in gelatinous-mediated export reflects a
773 redistribution of export production from existing sources, with the largest coming from small
774 mesozooplankton (Fig. 9a,c), as well as a reduction in the dissolved pool.

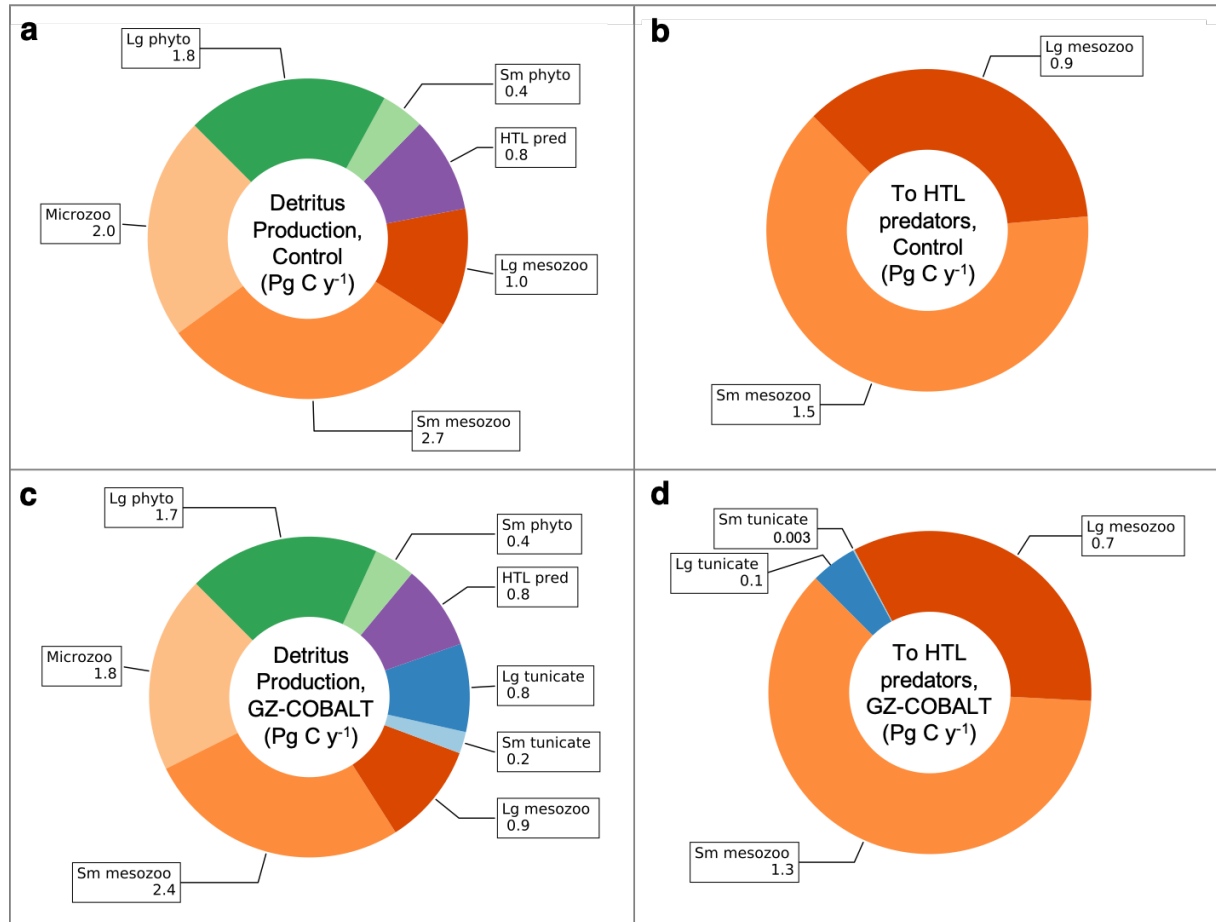
775
776



777
778
779
780

Figure 8. Differences in annual mean productivity ratios at the top 100 m between GZ-COBALT and the COBALTv2 control, showing ratios of microzooplankton production to NPP (a-c), mesozooplankton

781 production to NPP (d-f), POC export past 100 m to NPP, or pe-ratio (g-i), and free-living heterotrophic
 782 bacteria production to NPP (j-l). The plots show the GZ-COBALT simulation (left column; a,d,g,j), the
 783 COBALTv2 control (center column; b,e,h,k), and the difference between the two (right column; c,f,i,l).
 784



785 **Figure 9.** Top 100-m production of sinking detritus (a, c) and loss to higher trophic level (HTL) predators (b,
 786 d) in the COBALTv2 control (a, b) and GZ-COBALT (c, d) simulations. Of the total export production,
 787 approximately 84% of it sinks below 100 m. All values are from the top 100 m, and are in Pg C y⁻¹.
 788
 789

790 **Table 4.** Comparison of the major results from the COBALTv2 control, GZ-COBALT base simulation, and
 791 the sensitivity experiments. ‘z100’ refers to the top 100 m of the water column.
 792

Field	COBALT Control	GZ-COBALT Base	GZ-COBALT Sensitivity Experiments				
			Exp. 1	Exp. 2	Exp. 3	Exp. 4	Exp. 5
NPP (Pg C y ⁻¹)	55.4	53.7	55	51	54.5	54.5	53.6
Export at 100 m (Pg C y ⁻¹)	6.23	6.36	6.25	6.37	6.23	6.31	6.39
Total Grazing (Pg C y ⁻¹)	39.9	38.8	39.7	37.5	39.3	39.3	38.8
Zooplankton Ingestion, z100 (Pg C y ⁻¹)	53.6	51.1	53.1	47.9	52.2	52.4	50.9
HP Ingestion, z100 (Pg C y ⁻¹)	2.39	2.18	2.33	1.96	2.26	2.25	2.27
Total Phytoplankton Biomass (Pg C)	0.488	0.482	0.486	0.466	0.485	0.486	0.48
Total Zooplankton Biomass (Pg C)	0.659	0.719	0.659	0.676	0.706	0.677	0.766
Total Tunicate Biomass (Tg C)	---	102	8.69	112	73	36.9	161
Sm. Tunicate Biomass, z100 (Tg C)	---	5.78	6.13	37	3.73	3.2	5.53
Lg. Tunicate Biomass, z100 (Tg C)	---	81.5	1.08	61.5	58.1	26.8	132
Crustacean Mesozoop. Biomass (Pg C)	0.378	0.356	0.373	0.331	0.365	0.368	0.352
Tunicate Prod., z100 (Pg C y ⁻¹)	---	0.49	0.0361	1	0.259	0.0884	0.0724
Crust. Mesozoo. Prod., z100 (Pg C y ⁻¹)	4.54	3.89	4.39	3.31	4.14	4.21	2.77
Z-ratio	0.082	0.072	0.08	0.065	0.076	0.077	0.07
Sm. Tunicate Detritus Prod., z100 (Pg C y ⁻¹)	---	0.19	0.21	1.58	0.11	0.14	0.18
Lg. Tunicate Detritus Prod., z100 (Pg C y ⁻¹)	---	0.79	0.01	0.51	0.5	0.38	0.96
Tunicate Prod./Biomass, z100 (y ⁻¹)	---	5.61	5.02	10.2	4.19	2.95	5.25
Mesozoop Prod./Biomass, z100 (y ⁻¹)	14.70	13.4	14.3	12.3	13.9	14	13.1
Lg. Tunicate Prod. lost to HTL Pred.	---	57%	0%	56%	56%	51%	91%
Lg. Tunicate Prod. lost to Jelly-Falls	---	35%	4%	33%	34%	34%	0%
Slope of Sm. Tun/Chlorophyll scaling	---	0.89	0.9	1.1	0.67	0.79	0.88
Slope of Lg. Tun/Chlorophyll scaling	---	0.43	0.26	0.29	0.39	0.62	0.58

793
794

795 4. Discussion

796

797 We have added a simple representation of two pelagic tunicate groups, representing
798 appendicularians and thaliaceans, into the GFDL COBALTv2 ocean biogeochemistry model
799 (GZ-COBALT) that captures large-scale patterns in tunicate distribution consistent with the
800 emerging recognition of their importance to marine ecosystems, while maintaining a skillful
801 representation of crustacean mesozooplankton, surface chlorophyll, and macronutrient
802 concentrations. The GZ-COBALT simulation achieved a reasonable match between the
803 modelled mean tunicate biomass and a global observational dataset, compiled from a range of
804 sources including the COPEPOD database (O'Brien, 2014, 2005), Jellyfish Environmental
805 Database Initiative (JeDI) (Condon et al., 2015), and KRILLBASE (Atkinson et al., 2017).
806 Notably, GZ-COBALT captured a contrast between gelatinous and crustacean zooplankton types
807 in their emergent relationship between biomass and surface chlorophyll (Fig. 6). These results
808 confirm that it is possible to reconcile GZ biomass an order of magnitude above previous
809 estimates (Rensen et al., 2004) with prevalent crustacean zooplankton populations: carbon flows
810 through planktonic food-webs are sufficient to support both GZ and crustacean populations.

811 Observations of tunicate biomass exhibited high variability, even when compared with
812 crustacean zooplankton observations gridded to the same horizontal resolution (Moriarty and
813 O'Brien, 2013), which indicates either large sampling variability (e.g., from inconsistency in
814 sampling effort and/or gear), or unresolved physical or biological dynamics (Andersen, 1998;
815 Boero et al., 2008; d'Ovidio et al., 2010; Greer et al., 2020; Lévy et al., 2018; Luo et al., 2014),
816 or a combination thereof. The modelled variability for tunicates was lower than the observations
817 may suggest, even when daily rather than monthly outputs were sampled (Fig. S5). This was also
818 apparent for crustacean zooplankton, as it is a near-universal outcome when comparing global
819 biogeochemical fields against point measurements or averages of small numbers of point
820 measures (e.g., Krumhardt et al., 2017; Martiny et al., 2019; Saba et al., 2011; Usbeck et al.,
821 2003). The discrepancy is admittedly acute for the tunicates, which was not unexpected given the
822 sparsity and difficulty of measurements. A more complete understanding the drivers of this
823 patchiness and their implications will likely require high resolution physical simulations and GZ
824 models capable of better resolving unique aspects of GZ life cycles and ecology conducive to
825 patch formation (Groeneveld et al., 2020; Henschke et al., 2018a, 2018b)

826 In our analysis, we found a strong contrast in the biomass-chlorophyll relationship
827 between crustacean zooplankton, small tunicates, and large tunicates, wherein the large tunicates
828 exhibited a flatter scaling relationship compared to the steeper scalings of the small tunicates and
829 crustaceans (Fig. 6). After incorporating an expanded view of GZ biomass considering
830 undersampling by nets, the resultant observational biomass-chlorophyll scaling became one of
831 our primary validation tools, as this emergent relationship can capture the mean biomass
832 responses across productivity gradients. These relationships become important as steep spatial
833 gradients in the contemporary ocean generally translates to amplified trends with climate change
834 (Stock et al., 2017, 2014b). The shallower slope for large tunicates relative to crustacean
835 zooplankton, in contrast, is indicative of less sensitivity to NPP, and suggestive of greater
836 resilience to NPP declines projected by the majority of models under high emissions scenarios
837 (Kwiatkowski et al., 2020) than their crustacean competitors. This would be consistent with
838 current hypotheses for increased prevalence of GZ under climate change (Henschke et al., 2016).

839

840

841 *4.1 Marine food web and biogeochemical impacts*

842 Pelagic tunicates have long been identified as a potentially important source of carbon
843 export, due to fecal pellets from salps (Iversen et al., 2017; Madin et al., 2006; Ramaswamy et
844 al., 2005; Smith Jr et al., 2014; Urrère and Knauer, 1981) and appendicularians (Wilson et al.,
845 2013), discarded appendicularian houses (Berline et al., 2011; Lombard and Kjørboe, 2010;
846 Robison, 2005), and salp and pyrosome carcasses from jelly-falls (Henschke et al., 2013; Lebrato
847 et al., 2013; Lebrato and Jones, 2009). Given the boom-and-bust population dynamic of pelagic
848 tunicates, they can often be found to dominate POC export when present (Madin et al., 2006;
849 Smith Jr et al., 2014). Indeed, a recent study from a NASA EXPORTS cruise found that salp
850 fecal pellets comprised up to 80% of the detrital production in the upper 100 m in the NE Pacific
851 when present, though they contributed an average of 28% of fecal pellet carbon production over
852 a month-long sampling period (Stamieszkin et al., 2021). In our 20-year model climatology,
853 large tunicate detritus production comprises 20% of the total detritus production in the top 100 m
854 from July-September in the same region (Fig. S6). These values are a bit lower, but still fairly
855 consistent with the sampled cruise mean, though the high observed variability in Stamieszkin et
856 al. (2021) highlights the challenge in model-observation comparisons with snapshot studies at a
857 single time point. Model comparisons with GZ-COBALT and sediment trap data, which
858 integrates observations over longer time scales, will need to incorporate tunicate-specific POC
859 sinking speeds and is a target for future work.

860 One common implication of observations of pelagic tunicate-mediated carbon export is
861 that they would add to the existing POC export out of the surface ocean, often attributed to a
862 combination of phyto-detritus and crustacean zooplankton fecal pellets (Buesseler et al., 2008;
863 De La Rocha and Passow, 2007). Here, we found that when considering the upper oceans (top
864 100 m), the integration of pelagic tunicates with a “traditional” food-web model did not
865 substantially increase total export flux past 100 m, which was 6.36 Pg C y⁻¹ compared with 6.23
866 Pg C y⁻¹ in the COBALTv2 control despite GZ accounting for 0.7 Pg C y⁻¹. The integration of
867 GZ thus led primarily to a redistribution of fluxes away from those previously attributed to
868 crustacean zooplankton, rather than a creation of a new additive flux. The modest increase in
869 particle export that did occur is consistent with compensation for reductions in dissolved organic
870 carbon export arising from GZ-induced redirection of carbon flows away from the microbial
871 food-web (Fig. 8, 9).

872 Compared to the offline estimates of tunicate export (1.3-3.9 Pg C y⁻¹ at 100 m; Luo et
873 al., 2020), the online GZ-COBALT model was lower, suggesting that food web and
874 biogeochemical feedbacks decreased the overall export contribution of tunicates. Rather than
875 relying on the direct application of GZ data, GZ-COBALT accomplishes this correspondence by
876 mechanistically representing the primary observational features and satisfying myriad additional
877 physical, biogeochemical, and food-web constraints. Large tunicates contributed about four
878 times more export production than small tunicates in GZ-COBALT (0.79 vs. 0.19 Pg C y⁻¹), with
879 approximately 0.16 Pg C y⁻¹ from jelly-falls, which was only slightly lower than the offline
880 estimates of 0.3-0.7 Pg C y⁻¹. Tunicates in GZ-COBALT also contributed 0.1 Pg C y⁻¹ to higher
881 trophic level predators (Fig. 9d), which was much lower than the offline estimates of 0.8-1.1 Pg
882 C y⁻¹ (Luo et al., 2020). The higher trophic level predation in the offline model was one of the
883 least constrained parameters, as Luo et al. (2020) extracted a total GZ ecotrophic efficiency
884 (fraction of production to predation) from a combination of EcoPath models (e.g., Ruzicka et al.,
885 2020), and tuned this term for individual GZ groups to achieve a global fraction consistent with
886 EcoPath estimates. Future observational and experimental work aimed to increasing our

887 understanding of GZ predation by higher trophic levels should reduce the uncertainties
888 associated with these global models.

889 The GZ-COBALT simulation showed that, compared with the COBALTv2 control, the
890 largest impact of pelagic tunicates to ocean biogeochemical cycles is in the partitioning between
891 the biological pump and the microbial food web. In GZ-COBALT, the impact of tunicates served
892 to reduce microzooplankton and bacterial production as a function of NPP by 14% and 4%,
893 respectively (Fig. 8). Pelagic tunicates, unlike other gelatinous zooplankton, are notable for
894 primarily grazing on small particles and their high predator to prey size ratios (Conley et al.,
895 2018; Sutherland et al., 2010), though some exceptions exist (Post, 2002; Walters et al., 2019).
896 Recent work from Stukel et al. (2021) showed that in the Southern Ocean, the dominant salp, *S.*
897 *thompsoni*, most strongly competed with protistan grazers instead of with krill due to the large
898 size-based overlap between the salp and protistan diets. This is in contrast to previous
899 speculation that salps are a dominant competitor of the Antarctic krill, *Euphausia superba*, and
900 can be implicated as a factor in its long-term decline (Atkinson et al., 2004) and is consistent
901 with recent evidence that this decline can be attributed to positive anomalies in the Southern
902 Annular Mode (SAM) and loss of sea ice in the Southern Ocean (Atkinson et al., 2019). Our
903 results indicate that while tunicates do compete with large crustacean mesozooplankton for prey,
904 namely through the grazing of large phytoplankton and diatoms by appendicularians and
905 doliolids, tunicates also serve as a source of food for both small and large crustacean
906 mesozooplankton. Instead of competing with crustaceans, the magnitude of decline of
907 microzooplankton and heterotrophic bacteria production in GZ-COBALT compared to the
908 control and agreement with observations indicates that the microphagous tunicates serve as a
909 trophic and carbon export shunt away from the microbial loop and towards the mesozooplankton
910 food web and biological pump.

911 912 *4.2 Model limitations*

913 Amongst the marine zooplankton, thaliaceans are notable for their complex life cycles
914 which include the ability to reproduce asexually, alternation between sexual and asexual
915 reproductive phases (salps and doliolids), and hermaphroditism (pyrosomes), all of which can
916 yield large, transient, blooms under the right conditions (Andersen, 1998). Here, we have opted
917 against modeling the complex life cycle of pelagic tunicates (Henschke et al., 2018a, 2015;
918 Lombard et al., 2009b) for a more simple representation (Berline et al., 2011) aimed at capturing
919 their mean state, seasonal fluctuations, and long-term trends that can be run in an Earth System
920 Model over $O(100)$ years. As such, there were a number of necessary simplifications, and
921 associated insights.

922 The model suggests that the mean turnover time scale, as measured by the ratio of
923 production over biomass, or P/B, for pelagic tunicates is overall lower (implying slower growth)
924 than microzooplankton and crustacean mesozooplankton (Table 4, Fig. S7). While some shallow
925 coastal areas exhibited P/B exceeding $10\% \text{ d}^{-1}$ in the summer for both small and large tunicates,
926 the majority of the oceans had turnover rates $< 3\% \text{ d}^{-1}$, even in the summer months. In contrast,
927 the turnover timescales for large tunicates as reported in the literature were $15\text{-}71\% \text{ d}^{-1}$ (Deibel,
928 1982; Gibson and Paffenhöfer, 2000; Madin and Purcell, 1992). While there may be some
929 averaging due to the model's monthly output, not even daily data captured the range of
930 variability in the observations (Fig. S5). Future efforts may focus on determining whether the
931 model's inability to reproduce observed variability is due to its coarse horizontal resolution
932 relative to the scales of observed variations in tunicate distributions (Greer et al., 2021; Luo et

933 al., 2014), or due to the representation of the simplified life cycle. For some gelatinous
934 zooplankton populations, a representation of the complex life cycle may be key for reproducing
935 interannual and multi-decadal climate fluctuations (e.g., Henschke et al., 2018b).

936

937 *4.3 Future outlook*

938 Gelatinous zooplankton (GZ) are ubiquitous throughout the world's oceans and a key
939 contributor to marine food webs (Hays et al., 2018). Of the GZ, pelagic tunicates are likely the
940 most important group in terms of carbon fluxes, due to their low trophic position and
941 microphagous diet. We demonstrate, through a new model with food-web and biogeochemical
942 feedbacks incorporated, that it is possible to reconcile an enhanced role of GZ in marine food
943 webs with the established importance of crustacean mesozooplankton and other ocean
944 biogeochemical constraints. Simulation results provide GZ flux estimates arising from a self-
945 consistent physical-biological model satisfying myriad physical, biogeochemical and plankton
946 food-web constraints, a unique contribution relative to previous “offline” estimates. Climate
947 change is projected to drive decreases in NPP; coupled Model Intercomparison Project Phase 6
948 (CMIP6) models under the Shared Socioeconomic Pathway 5 (SSP5; fossil-fueled development)
949 project a 3-9% decline in NPP by the year 2100 (Kwiatkowski et al. 2020). Associated with
950 climate-induced NPP decreases, models also project a shift in mean pelagic body size: the
951 abundance of large autotrophic phytoplankton will likely be reduced relative to their smaller
952 counterparts due to increased warming, stratification, and subsequent nutrient limitation (Peter
953 and Sommer 2013). Consequently, as evidenced by the shallow scaling between biomass and
954 chlorophyll, the role of large pelagic tunicates (thaliaceans) in marine food webs may further
955 increase under climate change.

956 In this study, we have focused primarily on the upper ocean impacts of GZ, both to the
957 food web and to the balance between recycling and export. Omitted in this work are
958 considerations of the impact of fast sinking GZ export on the remineralization length scale and
959 transfer efficiency to “sequestration depths”, which may have further impacts on benthic fluxes
960 and air-sea CO₂ exchange (Kwon et al., 2009; Lebrato et al., 2019; Luo et al., 2020; Sweetman et
961 al., 2014; Titelman et al., 2006). In particular, there may be important feedbacks between
962 climate-induced stratification and tunicate-mediated increases in export. Our results indicate that
963 total carbon export was not significantly increased with inclusion of GZ in an ocean
964 biogeochemical model. However, these tunicate fluxes are globally quite significant and are
965 associated with a redistribution of export from existing phytoplankton and mesozooplankton
966 sources. As climate change will have differing impacts by taxonomic group, better understanding
967 of the sources of carbon export and the mechanisms that drive their variation will improve our
968 ability to project changes in the future.

969 **Acknowledgements**

970 We thank colleagues who have contributed to the development and integration of various
971 components of GFDL's Earth System Model that make this work possible, as well as the
972 technical support teams that maintain the NOAA/GFDL computing resources. JYL
973 acknowledges support from the NOAA's Marine Ecosystem Tipping Points Initiative. This work
974 also benefited from internal reviews by E. Drenkard and C. Schultz.

975

976 **Author contributions**

977 JYL and CAS conceived and designed the study, and evaluated the model. JYL wrote the code,
978 carried out simulations, analyzed data, and led the manuscript writing. JYL and TOB compiled
979 data. All authors contributed critical feedback and edits to the final manuscript.

980

981 **Competing Interests**

982 The authors have no competing interests to declare.

983

References

- Acuña, J.L., Kiefer, M., 2000. Functional response of the appendicularian *Oikopleura dioica*. *Limnol. Oceanogr.* 45, 608–618. <https://doi.org/10.4319/lo.2000.45.3.0608>
- Acuña, J.L., Lopez-Urrutia, A., Colin, S., 2011. Faking Giants: The Evolution of High Prey Clearance Rates in Jellyfishes. *Science* 333, 1627–1629. <https://doi.org/10.1126/Science.1205134>
- Adcroft, A., Anderson, W., Balaji, V., Blanton, C., Bushuk, M., Dufour, C.O., Dunne, J.P., Griffies, S.M., Hallberg, R., Harrison, M.J., Held, I.M., Jansen, M.F., John, J.G., Krasting, J.P., Langenhorst, A.R., Legg, S., Liang, Z., McHugh, C., Radhakrishnan, A., Reichl, B.G., Rosati, T., Samuels, B.L., Shao, A., Stouffer, R., Winton, M., Wittenberg, A.T., Xiang, B., Zadeh, N., Zhang, R., 2019. The GFDL Global Ocean and Sea Ice Model OM4.0: Model Description and Simulation Features. *J. Adv. Model. Earth Syst.* 11, 3167–3211. <https://doi.org/10.1029/2019MS001726>
- Allredge, A.L., 2005. The contribution of discarded appendicularian houses to the flux of particulate organic carbon from oceanic surface waters, in: Gorsky, G., Youngbluth, M.J., Deibel, D. (Eds.), *Response of Marine Ecosystems to Global Change: Ecological Impact of Appendicularians*. Éditions Scientifiques, Paris, pp. 309–326.
- Allredge, A.L., Silver, M.W., 1988. Characteristics, dynamics and significance of marine snow. *Progress in Oceanography* 20, 41–82. [https://doi.org/10.1016/0079-6611\(88\)90053-5](https://doi.org/10.1016/0079-6611(88)90053-5)
- Andersen, V., 1998. Salp and pyrosomid blooms and their importance in biogeochemical cycles, in: Bone, Q. (Ed.), *The Biology of Pelagic Tunicates*. Oxford University Press, New York, USA, pp. 125–137.
- Andersen, V., 1986. Effect of temperature on the filtration rate and percentage of assimilation of *Salpa fusiformis* Cuvier (Tunicata: Thaliacea). *Hydrobiologia* 137, 135–140.
- Atkinson, A., Hill, S.L., Pakhomov, E.A., Siegel, V., Anadon, R., Chiba, S., Daly, K.L., Downie, R., Fielding, S., Fretwell, P., Gerrish, L., Hosie, G.W., Jessopp, M.J., Kawaguchi, S., Krafft, B.A., Loeb, V., Nishikawa, J., Peat, H.J., Reiss, C.S., Ross, R.M., Quetin, L.B., Schmidt, K., Steinberg, D.K., Subramaniam, R.C., Tarling, G.A., Ward, P., 2017. KRILLBASE: A circumpolar database of Antarctic krill and salp numerical densities, 1926-2016. *Earth System Science Data*. <https://doi.org/10.5194/essd-9-193-2017>
- Atkinson, A., Hill, S.L., Pakhomov, E.A., Siegel, V., Reiss, C.S., Loeb, V.J., Steinberg, D.K., Schmidt, K., Tarling, G.A., Gerrish, L., Saille, S.F., 2019. Krill (*Euphausia superba*) distribution contracts southward during rapid regional warming. *Nature Clim Change* 9, 142–147. <https://doi.org/10.1038/s41558-018-0370-z>
- Atkinson, A., Siegel, V., Pakhomov, E., Rothery, P., 2004. Long-term decline in krill stock and increase in salps within the Southern Ocean. *Nature* 432, 100–103. <https://doi.org/10.1038/nature02996>
- Aumont, O., Ethé, C., Tagliabue, A., Bopp, L., Gehlen, M., 2015. PISCES-v2: An ocean biogeochemical model for carbon and ecosystem studies. *Geoscientific Model Development*. <https://doi.org/10.5194/gmd-8-2465-2015>
- Baker, A.R., Croot, P.L., 2010. Atmospheric and marine controls on aerosol iron solubility in seawater. *Marine Chemistry* 120, 4–13. <https://doi.org/10.1016/j.marchem.2008.09.003>
- Banse, K., 1992. Grazing, Temporal Changes of Phytoplankton Concentrations, and the Microbial Loop in the Open Sea, in: *Primary Productivity and Biogeochemical Cycles in the Sea*. https://doi.org/10.1007/978-1-4899-0762-2_22

- Berline, L., Stemmann, L., Vichi, M., Lombard, F., Gorsky, G., 2011. Impact of appendicularians on detritus and export fluxes: a model approach at DyFAMed site. *Journal of Plankton Research* 33, 855–872. <https://doi.org/10.1093/plankt/fbq163>
- Billett, D.S.M., Bett, B.J., Jacobs, C.L., Rouse, I.P., Wigham, B.D., 2006. Mass deposition of jellyfish in the deep Arabian Sea. *Limnology and Oceanography* 51, 2077–2083. <https://doi.org/10.4319/lo.2006.51.5.2077>
- Boero, F., Bouillon, J., Gravili, C., Miglietta, M.P., Parsons, T., Piraino, S., 2008. Gelatinous plankton: Irregularities rule the world (sometimes). *Marine Ecology Progress Series*. <https://doi.org/10.3354/meps07368>
- Buesseler, K.O., Trull, T.W., Steinberg, D.K., Silver, M.W., Siegel, D.A., Saitoh, S.-I., Lamborg, C.H., Lam, P.J., Karl, D.M., Jiao, N.Z., Honda, M.C., Elskens, M., Dehairs, F., Brown, S.L., Boyd, P.W., Bishop, J.K.B., Bidigare, R.R., 2008. VERTIGO (VERTical Transport In the Global Ocean): A study of particle sources and flux attenuation in the North Pacific. *Deep Sea Research Part II: Topical Studies in Oceanography* 55, 1522–1539. <https://doi.org/10.1016/j.dsr2.2008.04.024>
- Buitenhuis, E., Le Quéré, C., Aumont, O., Beaugrand, G., Bunker, A., Hirst, A., Ikeda, T., O'Brien, T., Piontkovski, S., Straile, D., 2006. Biogeochemical fluxes through mesozooplankton. *Global Biogeochem. Cycles* 20. <https://doi.org/10.1029/2005GB002511>
- Carlotti, F., Giske, J., Werner, F., 2000. Modeling zooplankton dynamics, in: Harris, R., Wiebe, P., Lenz, J., Skjoldal, H.R., Huntley, M. (Eds.), *ICES Zooplankton Methodology Manual*. Academic Press, London, pp. 571–667. <https://doi.org/10.1016/B978-012327645-2/50013-X>
- Condon, R.H., Graham, W.M., Duarte, C.M., Pitt, K.A., Lucas, C.H., Haddock, S.H.D., Sutherland, K.R., Robinson, K.L., Dawson, M.N., Decker, M.B., Mills, C.E., Purcell, J.E., Malej, A., Mianzan, H., Uye, S.I., Gelcich, S., Madin, L.P., 2012. Questioning the Rise of Gelatinous Zooplankton in the World's Oceans. *BioScience* 62, 160–169. <https://doi.org/10.1525/Bio.2012.62.2.9>
- Condon, R.H., Lucas, C.H., Duarte, C.M., Pitt, K.A., D., H.S.H., Madin, L.P., D., B.R., Sutherland K. R., Mianzan H. W., Purcell J. E., Decker M. B., Uye S.-I., Malej A., Bogeberg M., Everett J., Gibbons M., Gonzalez H., Hay S., Henschke, N., Hobson R. J., Kingsford M. J., Kremer P., Lehtiniemi M., Ohman M. D., Rissik D., Sheard K., Suthers I., Coleman N., Costello J.H., Gershwin L.A., Graham W.M., Robinson K.L., Richardson T.M., Giesecke R., Gorsky G., Greve W., Halsband-Lenk C., Hays G., Hobson V., Klein D., Lebrato, M., J., L., P., M., C., M., Perry G., Stemmann L., Sullivan B., Walker T., Schildhauer M., Regetz, J., 2015. Jellyfish Database Initiative (JeDI). <https://doi.org/10.1575/1912/7191>
- Conley, K.R., Lombard, F., Sutherland, K.R., 2018. Mammoth grazers on the ocean's minuteness: A review of selective feeding using mucous meshes, *Proceedings of the Royal Society B: Biological Sciences*. <https://doi.org/10.1098/rspb.2018.0056>
- d'Ovidio, F., De Monte, S., Alvain, S., Dandonneau, Y., Levy, M., 2010. Fluid dynamical niches of phytoplankton types. *Proceedings of the National Academy of Sciences* 107, 18366–18370. <https://doi.org/10.1073/pnas.1004620107>
- Dadon-Pilosof, A., Lombard, F., Genin, A., Sutherland, K.R., Yahel, G., 2019. Prey taxonomy rather than size determines salp diets. *Limnol Oceanogr* 64, 1996–2010. <https://doi.org/10.1002/lno.11165>

- De La Rocha, C.L., Passow, U., 2007. Factors influencing the sinking of POC and the efficiency of the biological carbon pump. *Deep Sea Research Part II: Topical Studies in Oceanography* 54, 639–658. <https://doi.org/10.1016/j.dsr2.2007.01.004>
- Deibel, D., 1998. Feeding and metabolism of Appendicularia, in: Bone, Q. (Ed.), *The Biology of Pelagic Tunicates*. Oxford University Press, New York, USA, pp. 139–149.
- Deibel, D., 1982. Laboratory determined mortality, fecundity and growth rates of *Thalia democratica* Forskal and *Dolioletta gegenbauri* Uljanin (Tunicata, Thaliacea). *Journal of Plankton Research* 4, 143–153. <https://doi.org/10.1093/plankt/4.1.143>
- Deibel, D., Lee, S., 1992. Retention efficiency of sub-micrometer particles by the pharyngeal filter of the pelagic tunicate *Oikopleura vanhoeffeni*. *Mar. Ecol. Prog. Ser.* 81, 25–30. <https://doi.org/10.3354/meps081025>
- Dubischar, C.D., Pakhomov, E.A., Bathmann, U.V., 2006. The tunicate *Salpa thompsoni* ecology in the Southern Ocean. II. Proximate and elemental composition. *Mar Biol* 149, 625–632. <https://doi.org/10.1007/s00227-005-0226-8>
- Dunne, J.P., Horowitz, L.W., Adcroft, A.J., Ginoux, P., Held, I.M., John, J.G., Krasting, J.P., Malyshev, S., Naik, V., Paulot, F., Shevliakova, E., Stock, C.A., Zadeh, N., Balaji, V., Blanton, C., Dunne, K.A., Dupuis, C., Durachta, J., Dussin, R., Gauthier, P.P.G., Griffies, S.M., Guo, H., Hallberg, R.W., Harrison, M., He, J., Hurlin, W., McHugh, C., Menzel, R., Milly, P.C.D., Nikonov, S., Paynter, D.J., Ploshay, J., Radhakrishnan, A., Rand, K., Reichl, B.G., Robinson, T., Schwarzkopf, D.M., Sentman, L.T., Underwood, S., Vahlenkamp, H., Winton, M., Wittenberg, A.T., Wyman, B., Zeng, Y., Zhao, M., 2020. The GFDL Earth System Model version 4.1 (GFDL-ESM 4.1): Overall coupled model description and simulation characteristics. *J. Adv. Model. Earth Syst.* <https://doi.org/10.1029/2019MS002015>
- Edwards, K.F., Thomas, M.K., Klausmeier, C.A., Litchman, E., 2015. Light and growth in marine phytoplankton: Allometric, taxonomic, and environmental variation. *Limnology and Oceanography*. <https://doi.org/10.1002/lno.10033>
- Edwards, K.F., Thomas, M.K., Klausmeier, C.A., Litchman, E., 2012. Allometric scaling and taxonomic variation in nutrient utilization traits and maximum growth rate of phytoplankton. *Limnology and Oceanography*. <https://doi.org/10.4319/lo.2012.57.2.0554>
- Eppley, R., 1972. Temperature and phytoplankton growth in the sea. *Fishery Bulletin*.
- Fasham, M.J.R., Ducklow, H.W., McKelvie, S.M., 1990. A nitrogen-based model of plankton dynamics in the oceanic mixed layer. *Journal of Marine Research*. <https://doi.org/10.1357/002224090784984678>
- Fernández, D., López-Urrutia, Á., Fernández, A., Acuña, J., Harris, R., 2004. Retention efficiency of 0.2 to 6 μm particles by the appendicularians *Oikopleura dioica* and *Fritillaria borealis*. *Mar. Ecol. Prog. Ser.* 266, 89–101. <https://doi.org/10.3354/meps266089>
- Flynn, K.J., 2005. Incorporating plankton respiration in models of aquatic ecosystem function, in: del Giorgio, P., Williams, P. (Eds.), *Respiration in Aquatic Ecosystems*. Oxford University Press, pp. 248–266. <https://doi.org/10.1093/acprof:oso/9780198527084.003.0013>
- García, H.E., Boyer, T.P., Locarnini, R.A., Antonov, J.I., Mishonov, A.V., Baranova, O.K., Zweng, M.M., Reagan, J.R., Johnson, D.R., 2013a. *World Ocean Atlas 2013. Volume 3: Dissolved oxygen, apparent oxygen utilization, and oxygen saturation*.

- Garcia, H.E., Locarnini, R.A., Boyer, T.P., Antonov, J.I., Baranova, O.K., Zweng, M.M., Reagan, J.R., Johnson, D.R., 2013b. World Ocean Atlas 2013, Volume 4 : Dissolved Inorganic Nutrients (phosphate, nitrate, silicate).
- Garcia, H.E., Weathers, K.W., Paver, C.R., Smolyar, I.V., Boyer, T.P., Locarnini, R.A., Zweng, M.M., Mishonov, A.V., Baranova, O.K., Seidov, D., Reagan, J.R., 2019. World Ocean Atlas 2018. Vol. 4: Dissolved Inorganic Nutrients (phosphate, nitrate and nitrate+nitrite, silicate).
- Gentleman, W., Leising, A., Frost, B., Strom, S., Murray, J., 2003. Functional responses for zooplankton feeding on multiple resources: A review of assumptions and biological dynamics. Deep-Sea Research Part II: Topical Studies in Oceanography. <https://doi.org/10.1016/j.dsr2.2003.07.001>
- Gibson, D.M., Paffenhöfer, G.-A., 2000. Feeding and growth rates of the doliolid, *Dolioletta gegenbauri* Uljanin (Tunicata, Thaliacea). Journal of Plankton Research 22, 1485–1500. <https://doi.org/10.1093/plankt/22.8.1485>
- Gorsky, G., Fenaux, R., 1998. The role of appendicularia in marine food webs, in: Bone, Q. (Ed.), The Biology of Pelagic Tunicates. Oxford University Press, New York, USA, pp. 161–169.
- Greer, A.T., Boyette, A.D., Cruz, V.J., Cambazoglu, M.K., Dzwonkowski, B., Chiaverano, L.M., Dykstra, S.L., Briseño-Avena, C., Cowen, R.K., Wiggert, J.D., 2020. Contrasting fine-scale distributional patterns of zooplankton driven by the formation of a diatom-dominated thin layer. Limnol Oceanogr 65, 2236–2258. <https://doi.org/10.1002/lno.11450>
- Greer, A.T., Chiaverano, L.M., Treible, L.M., Briseño-Avena, C., Hernandez, F.J., 2021. From spatial pattern to ecological process through imaging zooplankton interactions. ICES Journal of Marine Science fsab149. <https://doi.org/10.1093/icesjms/fsab149>
- Groeneveld, J., Berger, U., Henschke, N., Pakhomov, E.A., Reiss, C.S., Meyer, B., 2020. Blooms of a key grazer in the Southern Ocean – An individual-based model of *Salpa thompsoni*. Progress in Oceanography 185, 102339. <https://doi.org/10.1016/j.pocean.2020.102339>
- Hagadorn, J.W., Dott, R.H., Damrow, D., 2002. Stranded on a Late Cambrian shoreline: Medusae from central Wisconsin. Geology 30, 147–150.
- Hansen, B., Bjørnsen, P.K., Hansen, P.J., 1994. The size ratio between planktonic predators and their prey. Limnology and Oceanography 39, 395–403. <https://doi.org/10.4319/lo.1994.39.2.0395>
- Hansen, P.J., Bjørnsen, P.K., Hansen, B.W., 1997. Zooplankton grazing and growth: Scaling within the 2-2,000- μ m body size range. Limnology and Oceanography. <https://doi.org/10.4319/lo.1997.42.4.0687>
- Harbison, G.R., 1998. The parasites and predators of Thaliacea, in: Bone, Q. (Ed.), The Biology of Pelagic Tunicates. Oxford University Press, New York, USA, pp. 187–214.
- Harbison, G.R., McAlister, V.L., Gilmer, R.W., 1986. The Response of the Salp, *Pegea confoederata*, to High Levels of Particulate Material: Starvation in the Midst of Plenty. Limnology and Oceanography 31, 371–382.
- Hays, G.C., Doyle, T.K., Houghton, J.D.R., 2018. A Paradigm Shift in the Trophic Importance of Jellyfish?, Trends in Ecology and Evolution. <https://doi.org/10.1016/j.tree.2018.09.001>

- Henschke, N., Bowden, D.A., Everett, J.D., Holmes, S.P., Kloser, R.J., Lee, R.W., Suthers, I.M., 2013. Salp-falls in the Tasman Sea: a major food input to deep-sea benthos. *Marine Ecology Progress Series* 491, 165–175. <https://doi.org/10.3354/meps10450>
- Henschke, N., Everett, J.D., Richardson, A.J., Suthers, I.M., 2016. Rethinking the Role of Salps in the Ocean. *Trends in Ecology and Evolution* 31, 720–733. <https://doi.org/10.1016/j.tree.2016.06.007>
- Henschke, N., Pakhomov, E.A., 2019. Latitudinal variations in *Salpa thompsoni* reproductive fitness. *Limnol. Oceanogr.* 64, 575–584. <https://doi.org/10.1002/lno.11061>
- Henschke, N., Pakhomov, E.A., Groeneveld, J., Meyer, B., 2018a. Modelling the life cycle of *Salpa thompsoni*. *Ecological Modelling* 387, 17–26. <https://doi.org/10.1016/j.ecolmodel.2018.08.017>
- Henschke, N., Smith, J.A., Everett, J.D., Suthers, I.M., 2015. Population drivers of a *Thalia democratica* swarm: Insights from population modelling. *Journal of Plankton Research* 37, 1074–1087. <https://doi.org/10.1093/plankt/fbv024>
- Henschke, N., Stock, C.A., Sarmiento, J.L., 2018b. Modeling population dynamics of scyphozoan jellyfish (*Aurelia* spp.) in the Gulf of Mexico. *Marine Ecology Progress Series*. <https://doi.org/10.3354/meps12255>
- Hopcroft, R.R., Roff, J.C., 1998. Production of tropical larvaceans in Kingston Harbour, Jamaica: are we ignoring an important secondary producer? *J Plankton Res* 20, 557–569. <https://doi.org/10.1093/plankt/20.3.557>
- Horowitz, L.W., Walters, S., Mauzerall, D.L., Emmons, L.K., Rasch, P.J., Granier, C., Tie, X., Lamarque, J.-F., Schultz, M.G., Tyndall, G.S., Orlando, J.J., Brasseur, G.P., 2003. A global simulation of tropospheric ozone and related tracers: Description and evaluation of MOZART, version 2: MOZART-2 DESCRIPTION AND EVALUATION. *J. Geophys. Res.* 108, n/a-n/a. <https://doi.org/10.1029/2002JD002853>
- Iversen, M.H., Pakhomov, E.A., Hunt, B.P.V., van der Jagt, H., Wolf-Gladrow, D., Klaas, C., 2017. Sinkers or floaters? Contribution from salp pellets to the export flux during a large bloom event in the Southern Ocean. *Deep-Sea Research Part II: Topical Studies in Oceanography* 138, 116–125. <https://doi.org/10.1016/j.dsr2.2016.12.004>
- Johnson, R., Strutton, P.G., Wright, S.W., McMinn, A., Meiners, K.M., 2013. Three improved satellite chlorophyll algorithms for the Southern Ocean: SOUTHERN OCEAN CHLOROPHYLL ALGORITHMS. *J. Geophys. Res. Oceans* 118, 3694–3703. <https://doi.org/10.1002/jgrc.20270>
- Kearney, K.A., Bograd, S.J., Drenkard, E., Gomez, F.A., Haltuch, M., Hermann, A.J., Jacox, M.G., Kaplan, I.C., Koenigstein, S., Luo, J.Y., Masi, M., Muhling, B., Pozo Buil, M., Woodworth-Jefcoats, P.A., 2021. Using Global-Scale Earth System Models for Regional Fisheries Applications. *Front. Mar. Sci.* 8, 622206. <https://doi.org/10.3389/fmars.2021.622206>
- Kjørboe, T., Møhlenberg, F., Hamburger, K., 1985. Bioenergetics of the planktonic copepod *Acartia tonsa*: relation between feeding, egg production and respiration, and composition of specific dynamic action. *Mar. Ecol. Prog. Ser.* 26, 85–97. <https://doi.org/10.3354/meps026085>
- Krumhardt, K.M., Lovenduski, N.S., Iglesias-Rodriguez, M.D., Kleypas, J.A., 2017. Coccolithophore growth and calcification in a changing ocean. *Progress in Oceanography* 159, 276–295. <https://doi.org/10.1016/j.pocan.2017.10.007>

- Kwiatkowski, L., Torres, O., Bopp, L., Aumont, O., Chamberlain, M., R. Christian, J., P. Dunne, J., Gehlen, M., Ilyina, T., G. John, J., Lenton, A., Li, H., S. Lovenduski, N., C. Orr, J., Palmieri, J., Santana-Falcón, Y., Schwinger, J., Séférian, R., A. Stock, C., Tagliabue, A., Takano, Y., Tjiputra, J., Toyama, K., Tsujino, H., Watanabe, M., Yamamoto, A., Yool, A., Ziehn, T., 2020. Twenty-first century ocean warming, acidification, deoxygenation, and upper-ocean nutrient and primary production decline from CMIP6 model projections. *Biogeosciences* 17, 3439–3470. <https://doi.org/10.5194/bg-17-3439-2020>
- Kwon, E.Y., Primeau, F., Sarmiento, J.L., 2009. The impact of remineralization depth on the air–sea carbon balance. *Nature Geoscience* 2, 630–635. <https://doi.org/10.1038/ngeo612>
- Large, W.G., Yeager, S.G., 2009. The global climatology of an interannually varying air - Sea flux data set. *Climate Dynamics*. <https://doi.org/10.1007/s00382-008-0441-3>
- Lauvset, S.K., Key, R.M., Olsen, A., van Heuven, S., Velo, A., Lin, X., Schirnick, C., Kozyr, A., Tanhua, T., Hoppema, M., Jutterström, S., Steinfeldt, R., Jeansson, E., Ishii, M., Perez, F.F., Suzuki, T., Watelet, S., 2016. A new global interior ocean mapped climatology: the $1^\circ \times 1^\circ$ GLODAP version 2. *Earth Syst. Sci. Data* 8, 325–340. <https://doi.org/10.5194/essd-8-325-2016>
- Laval, P., 1980. Hyperiid Amphipods as Crustacean Parasitoids associated with Gelatinous Zooplankton, in: Barnes, M. (Ed.), *Oceanogr. Mar. Biol. Ann. Rev.* Aberdeen University Press, pp. 11–56.
- Lebrato, M., Jones, D.O.B., 2009. Mass deposition event of *Pyrosoma atlanticum* carcasses off Ivory Coast (West Africa). *Limnology and Oceanography* 54, 1197–1209. <https://doi.org/10.4319/lo.2009.54.4.1197>
- Lebrato, M., Molinero, J.C., Cartes, J.E., Lloris, D., Melin, F., Beni-Casadella, L., 2013. Sinking Jelly-Carbon Unveils Potential Environmental Variability along a Continental Margin. *PLoS ONE* 8, e82070. doi:10.1371/journal.pone.0082070. <https://doi.org/10.1371/journal.pone.0082070>
- Lebrato, M., Pahlow, M., Frost, J.R., Küter, M., Mendes, P.D.J., Molinero, J.C., Oschlies, A., 2019. Sinking of Gelatinous Zooplankton Biomass Increases Deep Carbon Transfer Efficiency Globally. *Global Biogeochemical Cycles* 33. <https://doi.org/10.1029/2019GB006265>
- Lebrato, M., Pitt, K., Sweetman, A.K., Jones, D., Cartes, J., Oschlies, A., Condon, R., Molinero, J., Adler, L., Gaillard, C., Lloris, D., Billett, D., 2012. Jelly-falls historic and recent observations: a review to drive future research directions. *Hydrobiologia* 690, 227–245. <https://doi.org/10.1007/s10750-012-1046-8>
- Lévy, M., Franks, P.J.S., Smith, K.S., 2018. The role of submesoscale currents in structuring marine ecosystems. *Nat Commun* 9, 4758. <https://doi.org/10.1038/s41467-018-07059-3>
- Llopiz, J.K., Richardson, D.E., Shiroza, A., Smith, S.L., Cowen, R.K., 2010. Distinctions in the diets and distributions of larval tunas and the important role of appendicularians. *Limnology and Oceanography* 55, 983–996. <https://doi.org/10.4319/lo.2010.55.3.0983>
- Locarnini, R.A., Mishonov, A.V., Antonov, J.I., Boyer, T.P., Garcia, H.E., Baranova, O.K., Zweng, M.M., Paver, C.R., Reagan, J.R., Johnson, D.R., Hamilton, M., Seidov, D., 2013. *World Ocean Atlas 2013, Volume 1: Temperature*.
- Lombard, F., Kiørboe, T., 2010. Marine snow originating from appendicularian houses: Age-dependent settling characteristics. *Deep Sea Research Part I: Oceanographic Research Papers* 57, 1304–1313. <https://doi.org/10.1016/j.dsr.2010.06.008>

- Lombard, F., Renaud, F., Sainsbury, C., Sciandra, A., Gorsky, G., 2009a. Appendicularian ecophysiology I. Food concentration dependent clearance rate, assimilation efficiency, growth and reproduction of *Oikopleura dioica*. *Journal of Marine Systems*. <https://doi.org/10.1016/j.jmarsys.2009.01.004>
- Lombard, F., Sciandra, A., Gorsky, G., 2009b. Appendicularian ecophysiology. II. Modeling nutrition, metabolism, growth and reproduction of the appendicularian *Oikopleura dioica*. *Journal of Marine Systems*. <https://doi.org/10.1016/j.jmarsys.2009.01.005>
- Lombard, F., Sciandra, A., Gorsky, G., 2005. Influence of body mass, food concentration, temperature and filtering activity on the oxygen uptake of the appendicularian *Oikopleura dioica*. *Marine Ecology Progress Series*. <https://doi.org/10.3354/meps301149>
- Lombard, F., Selander, E., Kiørboe, T., 2011. Active prey rejection in the filter-feeding appendicularian *Oikopleura dioica*. *Limnol. Oceanogr.* 56, 1504–1512. <https://doi.org/10.4319/lo.2011.56.4.1504>
- Lucas, C.H., Dawson, M.N., 2014. What Are Jellyfishes and Thaliaceans and Why Do They Bloom?, in: Pitt, K.A., Lucas, C.H. (Eds.), *Jellyfish Blooms*. Springer Netherlands, pp. 9–44. https://doi.org/10.1007/978-94-007-7015-7_2
- Lucas, C.H., Jones, D.O.B., Hollyhead, C.J., Condon, R.H., Duarte, C.M., Graham, W.M., Robinson, K.L., Pitt, K.A., Schildhauer, M., Regetz, J., 2014. Gelatinous zooplankton biomass in the global oceans: geographic variation and environmental drivers. *Global Ecology and Biogeography* 23, 701–714. <https://doi.org/10.1111/geb.12169>
- Luo, J.Y., Condon, R.H., Stock, C.A., Duarte, C.M., Lucas, C.H., Pitt, K.A., Cowen, R.K., 2020. Gelatinous zooplankton-mediated carbon flows in the global oceans: A data-driven modeling study. *Global Biogeochemical Cycles*. <https://doi.org/10.1029/2020GB006704>
- Luo, J.Y., Grassian, B., Tang, D., Irissou, J.-O., Greer, A.T., Guigand, C.M., McClatchie, S., Cowen, R.K., 2014. Environmental drivers of the fine-scale distribution of a gelatinous zooplankton community across a mesoscale front. *Marine Ecology Progress Series* 510, 129–149. <https://doi.org/10.3354/meps10908>
- Lynam, C.P., Gibbons, M.J., Axelsen, B.E., Sparks, C.A.J., Coetzee, J., Heywood, B.G., Brierley, A.S., 2006. Jellyfish overtake fish in a heavily fished ecosystem. *Current Biology* 16, R492–R493. <https://doi.org/10.1016/j.cub.2006.06.018>
- Madin, L.P., Deibel, D., 1998. Feeding and energetics of Thaliacea, in: Bone, Q. (Ed.), *The Biology of Pelagic Tunicates*. Oxford University Press, New York, USA, pp. 81–103.
- Madin, L.P., Harbison, G.R., 1977. The associations of Amphipoda Hyperiidea with gelatinous zooplankton—I. Associations with Salpidae. *Deep Sea Research* 24, 449–463. [https://doi.org/10.1016/0146-6291\(77\)90483-0](https://doi.org/10.1016/0146-6291(77)90483-0)
- Madin, L.P., Kremer, P., Wiebe, P.H., Purcell, J.E., Horgan, E.H., Nemazie, D.A., 2006. Periodic swarms of the salp *Salpa aspera* in the Slope Water off the NE United States: Biovolume, vertical migration, grazing, and vertical flux. *Deep-Sea Research Part I-Oceanographic Research Papers* 53, 804–819. <https://doi.org/10.1016/j.dsr.2005.12.018>
- Madin, L.P., Purcell, J.E., 1992. Feeding, metabolism, and growth of *Cyclosalpa bakeri* in the subarctic Pacific. *Limnology and Oceanography* 37, 1236–1251. <https://doi.org/10.4319/lo.1992.37.6.1236>
- Martiny, A.C., Lomas, M.W., Fu, W., Boyd, P.W., Chen, Y.L., Cutter, G.A., Ellwood, M.J., Furuya, K., Hashihama, F., Kanda, J., Karl, D.M., Kodama, T., Li, Q.P., Ma, J., Moutin, T., Woodward, E.M.S., Moore, J.K., 2019. Biogeochemical controls of surface ocean phosphate. *Sci. Adv.* 5, eaax0341. <https://doi.org/10.1126/sciadv.aax0341>

- Mayzaud, P., Boutoute, M., Gasparini, S., Mousseau, L., Lefevre, D., 2005. Respiration in marine zooplankton - The other side of the coin: CO₂ production. *Limnology and Oceanography*. <https://doi.org/10.4319/lo.2005.50.1.0291>
- Mayzaud, P., Boutoute, M., Perissinotto, R., Nichols, P., 2007. Polar and Neutral Lipid Composition in the Pelagic Tunicate *Pyrosoma atlanticum*. *Lipids* 42, 647–657. <https://doi.org/10.1007/s11745-007-3066-0>
- Mianzan, H., Pájaro, M., Colombo, G.A., Madirolas, A., 2001. Feeding on survival-food: gelatinous plankton as a source of food for anchovies. *Hydrobiologia* 451, 45–53.
- Moriarty, R., O'Brien, T.D., 2013. Distribution of mesozooplankton biomass in the global ocean. *Earth System Science Data* 5, 45–55. <https://doi.org/10.5194/essd-5-45-2013>
- Munk, W., Riley, G., 1952. Absorption of nutrients by aquatic plants. *J. Mar. Res.* 11, 215–240.
- Muxagata, E., 1999. Avaliação da biomassa e distribuição zooplanctônica na plataforma continental sudeste brasileira durante o inverno de 1995 (Evaluation of the biomass and distribution of the zooplankton in the southeastern continental shelf of Brazil during the winter of 1995) (M.Sc Thesis). Departamento de Oceanografia - Universidade Federal de Rio Grande (FURG), Rio Grande, Brazil.
- O'Brien, T.D., 2014. COPEPOD: The Global Plankton Database. An overview of the 2014 database contents, processing methods, and access interface. (NOAA Tech. Memo. No. NMFS-F/ST-37). U.S. Dept. of Commerce.
- O'Brien, T.D., 2005. COPEPOD: A Global Plankton Database. A review of the 2005 database contents and creation of new global zooplankton biomass fields. (NOAA Tech. Memo. No. NMFS-F/SPO-73). U.S. Dept. of Commerce.
- Paffenhöfer, G.-A., Köster, M., 2011. From one to many: on the life cycle of *Dolioletta gegenbauri* Uljanin (Tunicata, Thaliacea). *Journal of Plankton Research* 33, 1139–1145. <https://doi.org/10.1093/plankt/fbr001>
- Pakhomov, E.A., 2004. Salp/krill interactions in the eastern Atlantic sector of the Southern Ocean. *Deep Sea Research Part II: Topical Studies in Oceanography, The SWEDARP 1997/98 Expedition* 51, 2645–2660. <https://doi.org/10.1016/j.dsr2.2001.03.001>
- Pakhomov, E.A., Dubischar, C.D., Strass, V., Brichta, M., Bathmann, U.V., 2006. The tunicate *Salpa thompsoni* ecology in the Southern Ocean. I. Distribution, biomass, demography and feeding ecophysiology. *Marine Biology* 149, 609–623.
- Perissinotto, R., Pakhomov, E.A., 1998. Contribution of salps to carbon flux of marginal ice zone of the Lazarev Sea, Southern Ocean. *Marine Biology* 131, 25–32.
- Pershing, A.J., Stamieszkin, K., 2020. The North Atlantic Ecosystem, from Plankton to Whales. *Annu. Rev. Mar. Sci.* 12, 339–359. <https://doi.org/10.1146/annurev-marine-010419-010752>
- Post, D.M., 2002. Using stable isotopes to estimate trophic position: Models, methods, and assumptions. *Ecology* 83, 703–718.
- Purcell, J.E., Sturdevant, M.V., Galt, C.P., 2005. A review of appendicularians as prey of fish and invertebrate predators, in: Gorsky, G., Youngbluth, M.J., Diebel, D. (Eds.), *Response of Marine Ecosystems to Global Change: Ecological Impact of Appendicularians*. Contemporary Publishing International, Paris, France, pp. 359–435.
- Ramaswamy, V., Sarin, M.M., Rengarajan, R., 2005. Enhanced export of carbon by salps during the northeast monsoon period in the northern Arabian Sea. *Deep Sea Research Part II: Topical Studies in Oceanography* 52, 1922–1929. <http://dx.doi.org/10.1016/j.dsr2.2005.05.005>

- Remsen, A., Hopkins, T.L., Samson, S., 2004. What you see is not what you catch: a comparison of concurrently collected net, Optical Plankton Counter, and Shadowed Image Particle Profiling Evaluation Recorder data from the northeast Gulf of Mexico. *Deep-Sea Research Part I: Oceanographic Research Papers* 51, 129–151. <https://doi.org/10.1016/j.dsr.2003.09.008>
- Robison, B.H., 2005. Giant Larvacean Houses: Rapid Carbon Transport to the Deep Sea Floor. *Science* 308, 1609–1611. <https://doi.org/10.1126/science.1109104>
- Ruzicka, J., Brodeur, R.D., Ciciel, K., Decker, M.B., 2020. Examining the ecological role of jellyfish in the Eastern Bering Sea. *ICES Journal of Marine Science* 77, 791–802. <https://doi.org/10.1093/icesjms/fsz244>
- Saba, V.S., Friedrichs, M.A.M., Antoine, D., Armstrong, R.A., Asanuma, I., Behrenfeld, M.J., Ciotti, A.M., Dowell, M., Hoepffner, N., Hyde, K.J.W., Ishizaka, J., Kameda, T., Marra, J., Mlin, F., Morel, A., O'Reilly, J., Scardi, M., Smith, W.O., Smyth, T.J., Tang, S., Uitz, J., Waters, K., Westberry, T.K., 2011. An evaluation of ocean color model estimates of marine primary productivity in coastal and pelagic regions across the globe. *Biogeosciences*. <https://doi.org/10.5194/bg-8-489-2011>
- Seitzinger, S.P., Harrison, J.A., Dumont, E., Beusen, A.H.W., Bouwman, A.F., 2005. Sources and delivery of carbon, nitrogen, and phosphorus to the coastal zone: An overview of Global Nutrient Export from Watersheds (NEWS) models and their application: GLOBAL EXPORT OF C, N, AND P TO COASTAL SYSTEMS. *Global Biogeochem. Cycles* 19, n/a-n/a. <https://doi.org/10.1029/2005GB002606>
- Smith Jr, K.L., Sherman, A.D., Huffard, C.L., McGill, P.R., Henthorn, R., Von Thun, S., Ruhl, H.A., Kahru, M., Ohman, M.D., 2014. Large salp bloom export from the upper ocean and benthic community response in the abyssal northeast Pacific: Day to week resolution. *Limnol. Oceanogr* 59, 745–757.
- Stamieszkin, K., Steinberg, D.K., Maas, A.E., 2021. Fecal pellet production by mesozooplankton in the subarctic Northeast Pacific Ocean. *Limnol Oceanogr* 66, 2585–2597. <https://doi.org/10.1002/lno.11774>
- Steinberg, D.K., Cope, J.S., Wilson, S.E., Kobari, T., 2008. A comparison of mesopelagic mesozooplankton community structure in the subtropical and subarctic North Pacific Ocean. *Deep Sea Research Part II: Topical Studies in Oceanography* 55, 1615–1635. <https://doi.org/10.1016/j.dsr2.2008.04.025>
- Steinberg, D.K., Ruck, K.E., Gleiber, M.R., Garzio, L.M., Cope, J.S., Bernard, K.S., Stammerjohn, S.E., Schofield, O.M.E., Quetin, L.B., Ross, R.M., 2015. Long-term (1993–2013) changes in macrozooplankton off the Western Antarctic Peninsula. *Deep Sea Research Part I: Oceanographic Research Papers* 101, 54–70. <http://dx.doi.org/10.1016/j.dsr.2015.02.009>
- Stock, C.A., Dunne, J.P., 2010. Controls on the ratio of mesozooplankton production to primary production in marine ecosystems. *Deep-Sea Research Part I: Oceanographic Research Papers*. <https://doi.org/10.1016/j.dsr.2009.10.006>
- Stock, C.A., Dunne, J.P., Fan, S., Ginoux, P., John, J., Krasting, J.P., Laufkötter, C., Paulot, F., Zadeh, N., 2020. Ocean Biogeochemistry in GFDL's Earth System Model 4.1 and Its Response to Increasing Atmospheric CO₂. *J. Adv. Model. Earth Syst.* 12. <https://doi.org/10.1029/2019MS002043>

- Stock, C.A., Dunne, J.P., John, J.G., 2014a. Global-scale carbon and energy flows through the marine planktonic food web: An analysis with a coupled physical–biological model. *Progress in Oceanography* 120, 1–28. <http://dx.doi.org/10.1016/j.pocean.2013.07.001>
- Stock, C.A., Dunne, J.P., John, J.G., 2014b. Drivers of trophic amplification of ocean productivity trends in a changing climate. *Biogeosciences*. <https://doi.org/10.5194/bg-11-7125-2014>
- Stock, C.A., John, J.G., Rykaczewski, R.R., Asch, R.G., Cheung, W.W.L., Dunne, J.P., Friedland, K.D., Lam, V.W.Y., Sarmiento, J.L., Watson, R.A., 2017. Reconciling fisheries catch and ocean productivity. *Proceedings of the National Academy of Sciences* 201610238. <https://doi.org/10.1073/pnas.1610238114>
- Stock, C.A., Powell, T.M., Levin, S.A., 2008. Bottom-up and top-down forcing in a simple size-structured plankton dynamics model. *Journal of Marine Systems* 74, 134–152. <https://doi.org/10.1016/j.jmarsys.2007.12.004>
- Stukel, M.R., Décima, M., Selph, K.E., Gutiérrez-Rodríguez, A., 2021. Size-specific grazing and competitive interactions between large salps and protistan grazers. *Limnol Oceanogr* 66, 2521–2534. <https://doi.org/10.1002/lno.11770>
- Sutherland, K.R., Madin, L.P., Stocker, R., 2010. Filtration of submicrometer particles by pelagic tunicates. *Proceedings of the National Academy of Sciences* 107, 15129–15134. <https://doi.org/10.1073/pnas.1003599107>
- Sweetman, A.K., Smith, C.R., Dale, T., Jones, D.O.B., 2014. Rapid scavenging of jellyfish carcasses reveals the importance of gelatinous material to deep-sea food webs. *Proceedings of the Royal Society B-Biological Sciences* 281. <https://doi.org/Artn20142210> 10.1098/Rspb.2014.2210
- Takahashi, K., Ichikawa, T., Saito, H., Takehi, S., Sugimoto, Y., Hidaka, K., Hamasaki, K., 2013. Sapphirinid copepods as predators of doliolids: Their role in doliolid mortality and sinking flux. *Limnology and Oceanography* 58, 1972–1984. <https://doi.org/10.4319/lno.2013.58.6.1972>
- Titelman, J., Riemann, L., Sørnes, T.A., Nilsen, T., Griekspoor, P., B'aaamstedt, U., 2006. Turnover of dead jellyfish: Stimulation and retardation of microbial activity. *Marine Ecology Progress Series* 325, 43–58.
- Trueman, E., Bone, Q., Braconnot, J., 1984. Oxygen consumption in swimming salps (tunicata: thaliacea). *Journal of Experimental Biology*.
- Turner, J.T., 2015. Zooplankton fecal pellets, marine snow, phytodetritus and the ocean's biological pump. *Progress in Oceanography* 130, 205–248. <https://doi.org/10.1016/j.pocean.2014.08.005>
- Urrère, M.A., Knauer, G.A., 1981. Zooplankton fecal pellet fluxes and vertical transport of particulate organic material in the pelagic environment. *Journal of Plankton Research* 3, 369–387.
- Usbeck, R., Schlitzer, R., Fischer, G., Wefer, G., 2003. Particle fluxes in the ocean: comparison of sediment trap data with results from inverse modeling. *Journal of Marine Systems* 39, 167–183. [https://doi.org/10.1016/S0924-7963\(03\)00029-0](https://doi.org/10.1016/S0924-7963(03)00029-0)
- Vargas, C.A., Madin, L.P., 2004. Zooplankton feeding ecology: clearance and ingestion rates of the salps *Thalia democratica*, *Cyclosalpa affinis* and *Salpa cylindrica* on naturally occurring particles in the Mid-Atlantic Bight. *Journal of Plankton Research* 26, 827–833. <https://doi.org/10.1093/plankt/fbh068>

- Verity, P., Smetacek, V., 1996. Organism life cycles, predation, and the structure of marine pelagic ecosystems. *Mar. Ecol. Prog. Ser.* 130, 277–293. <https://doi.org/10.3354/meps130277>
- Waite, A., Bienfang, P.K., Harrison, P.J., 1992. Spring bloom sedimentation in a subarctic ecosystem. *Marine Biology* 114, 131–138. <https://doi.org/10.1007/BF00350862>
- Walters, T.L., Lamboley, L.M., López-Figueroa, N.B., Rodríguez-Santiago, Á.E., Gibson, D.M., Frischer, M.E., 2019. Diet and trophic interactions of a circumglobally significant gelatinous marine zooplankton, *Doliolletta gegenbauri* (Uljanin, 1884). *Mol Ecol* 28, 176–189. <https://doi.org/10.1111/mec.14926>
- Ward, B.A., Dutkiewicz, S., Jahn, O., Follows, M.J., 2012. A size-structured food-web model for the global ocean. *Limnology and Oceanography*. <https://doi.org/10.4319/lo.2012.57.6.1877>
- Wiebe, P.H., Benfield, M.C., 2003. From the Hensen net toward four-dimensional biological oceanography. *Progress in Oceanography* 56, 7–136. [https://doi.org/10.1016/S0079-6611\(02\)00140-4](https://doi.org/10.1016/S0079-6611(02)00140-4)
- Wilson, S.E., Ruhl, H.A., Smith Jr, K.L., 2013. Zooplankton fecal pellet flux in the abyssal northeast Pacific: A 15 year time-series study. *Limnology and Oceanography* 58, 881–892. <https://doi.org/10.4319/lo.2013.58.3.0881>
- Wright, R.M., Le Quéré, C., Buitenhuis, E., Pitois, S., Gibbons, M.J., 2021. Role of jellyfish in the plankton ecosystem revealed using a global ocean biogeochemical model. *Biogeosciences* 18, 1291–1320. <https://doi.org/10.5194/bg-18-1291-2021>
- Zhao, M., Golaz, J.-C., Held, I.M., Guo, H., Balaji, V., Benson, R., Chen, J.-H., Chen, X., Donner, L.J., Dunne, J.P., Dunne, K., Durachta, J., Fan, S.-M., Freidenreich, S.M., Garner, S.T., Ginoux, P., Harris, L.M., Horowitz, L.W., Krasting, J.P., Langenhorst, A.R., Liang, Z., Lin, P., Lin, S.-J., Malyshev, S.L., Mason, E., Milly, P.C.D., Ming, Y., Naik, V., Paulot, F., Paynter, D., Phillipps, P., Radhakrishnan, A., Ramaswamy, V., Robinson, T., Schwarzkopf, D., Seman, C.J., Shevliakova, E., Shen, Z., Shin, H., Silvers, L.G., Wilson, J.R., Winton, M., Wittenberg, A.T., Wyman, B., Xiang, B., 2018. The GFDL Global Atmosphere and Land Model AM4.0/LM4.0: 2. Model Description, Sensitivity Studies, and Tuning Strategies. *J. Adv. Model. Earth Syst.* 10, 735–769. <https://doi.org/10.1002/2017MS001209>
- Zweng, M.M., Reagan, J.R., Antonov, J.I., Locarnini, R.A., Mishonov, A.V., Boyer, T.P., Garcia, H.E., Baranova, O.K., Johnson, D.R., Siedov, D., Biddle, M.M., 2013. *World Ocean Atlas 2013, Volume 2: Salinity*.

Supplemental Tables and Figures

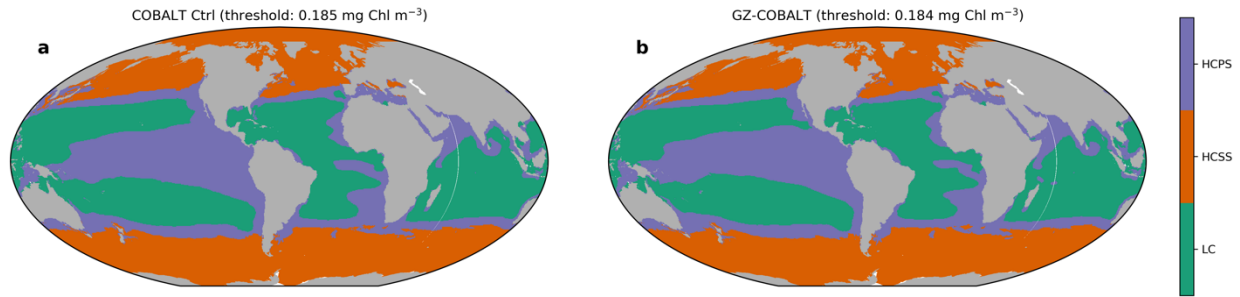


Figure S1. Major ocean biomes for the COBALTv2 control (a) and GZ-COBALT (b). The chlorophyll thresholds delineating the low chlorophyll (LC) regions were 0.162 and 0.184 mg Chl m⁻³ for the control and GZ-COBALT, respectively. The annual minimum of the mixed layer depth irradiance climatology (< 5 W m⁻²) delineated the high chlorophyll seasonally stratified (HCSS) biome from the high chlorophyll permanently stratified (HCPS) biome.

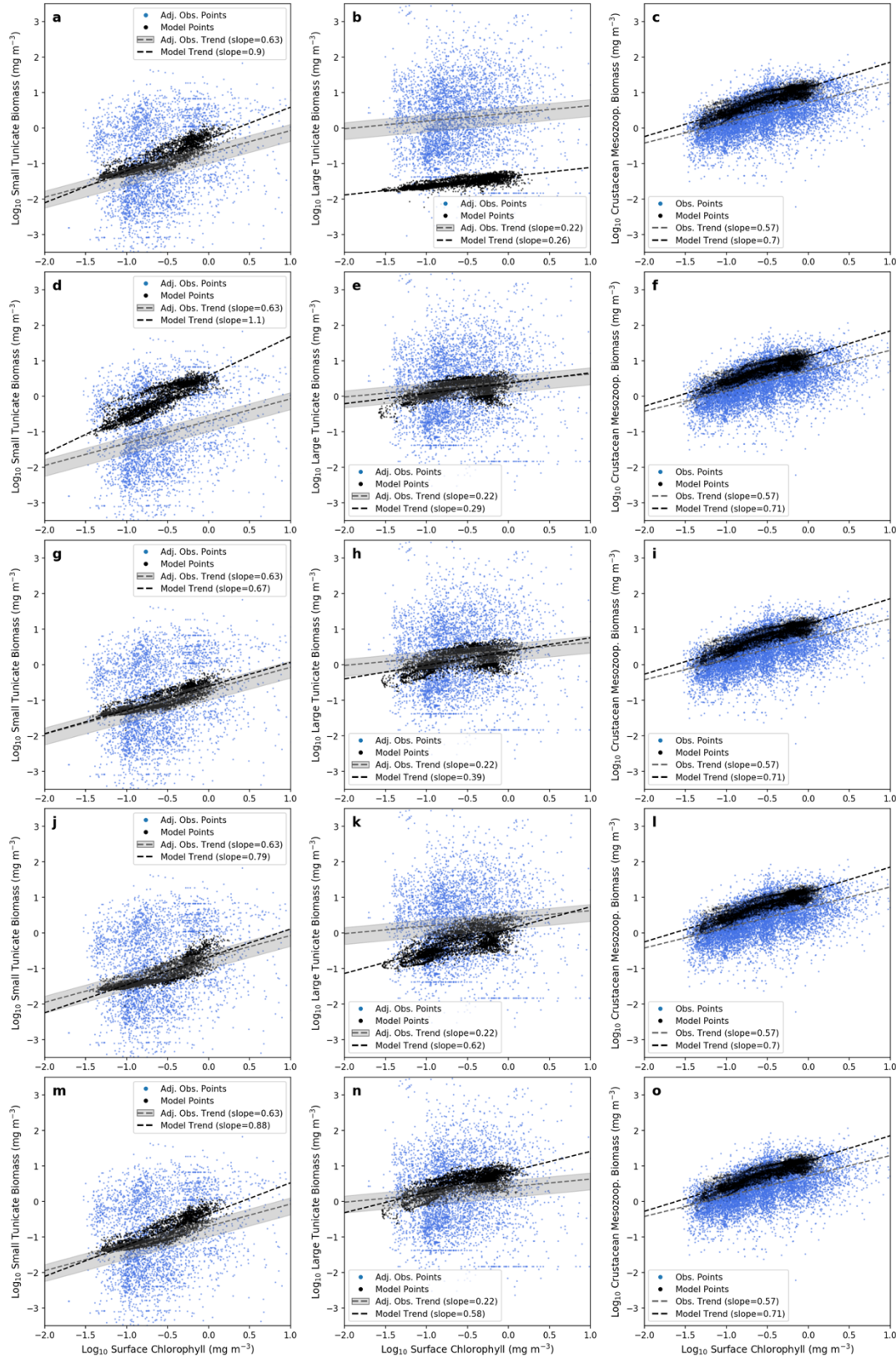


Figure S2. Biomass chlorophyll scaling for small tunicates (left column), large tunicates (center column) and crustacean mesozooplankton (right column) for the five sensitivity cases: case 1 (a-c), where large

tunicate basal respiration is increased; case 2 (d-f), where small tunicate maximum ingestion rate is increased; case 3 (g-i), where the tunicate ingestion half-saturation constant is the same as crustaceans, and maximum ingestion is adjusted accordingly; case 4 (j-l), where tunicate assimilation efficiency is set to be a constant; and case 5 (m-o), where large tunicate aggregation mortality is turned off. See Table 2, and the caption on Fig. 6 for further details.

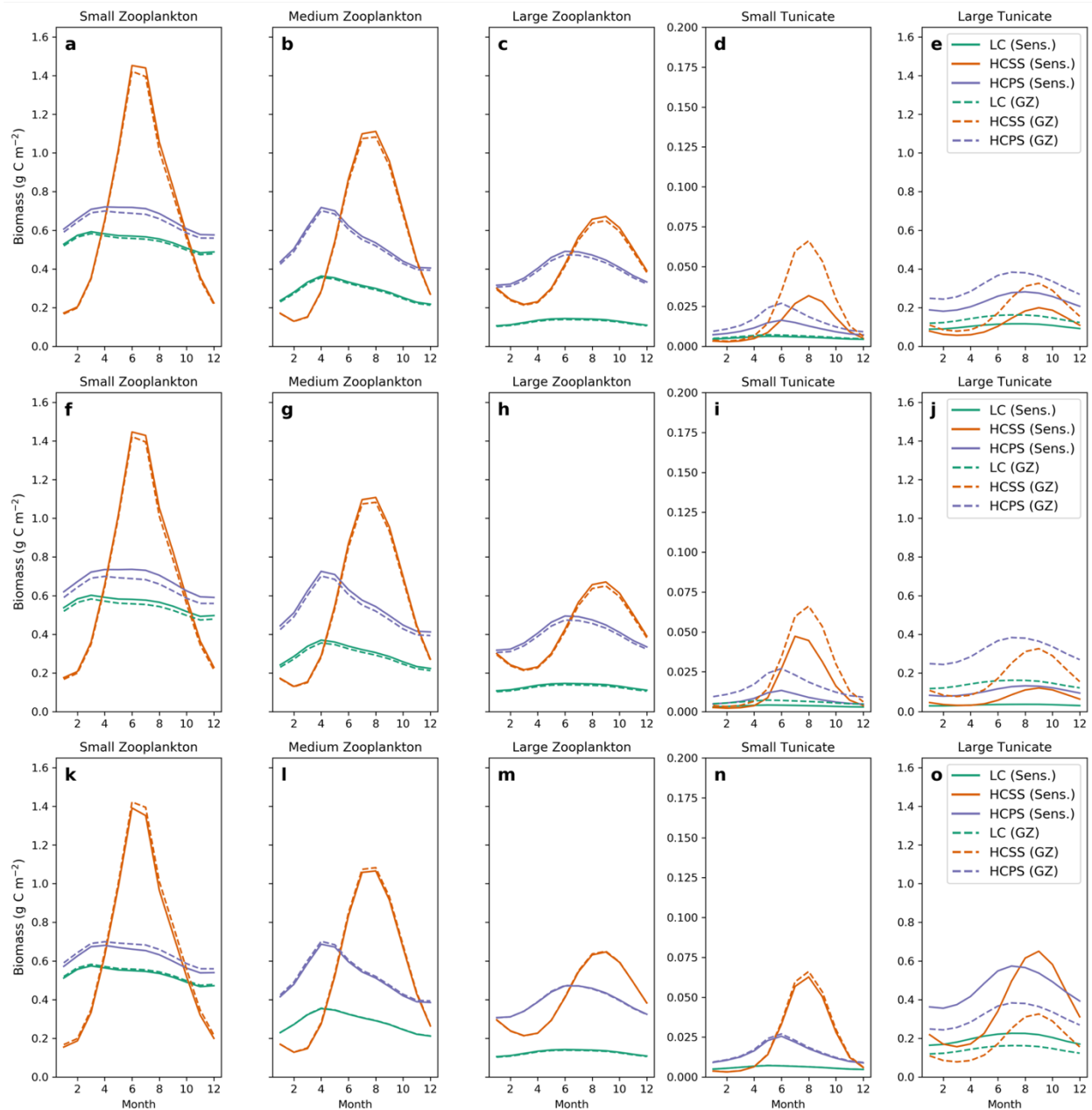


Figure S3. Zooplankton seasonal cycle differences between the GZ-COBALT base case (dashed) and three of the sensitivity cases: case 3 (a-e); case 4 (f-j); case 5 (k-o). See caption on Fig. 7 for further details.

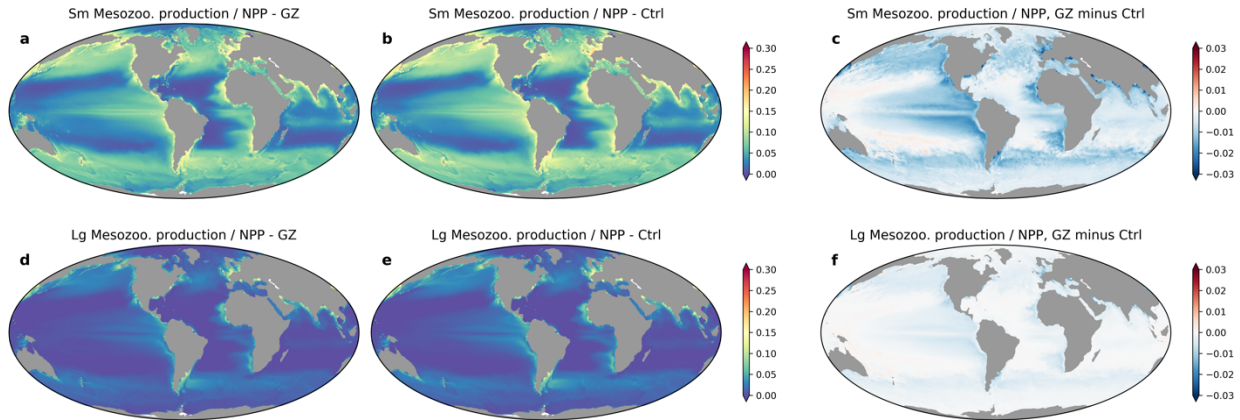


Figure S4. Differences in annual mean productivity ratios at the top 100 m between GZ-COBALT and the COBALTv2 control, showing ratios of small mesozooplankton (= medium zooplankton) production to NPP (a-c) and large mesozooplankton (= large zooplankton) production to NPP (d-f). The plots show the GZ-COBALT simulation (left column; a, d), the COBALTv2 control (center column; b, e), and the difference between the two (right column; c, f). Colorbar is set to be the same as in Fig. 8 to allow for a direct comparison.

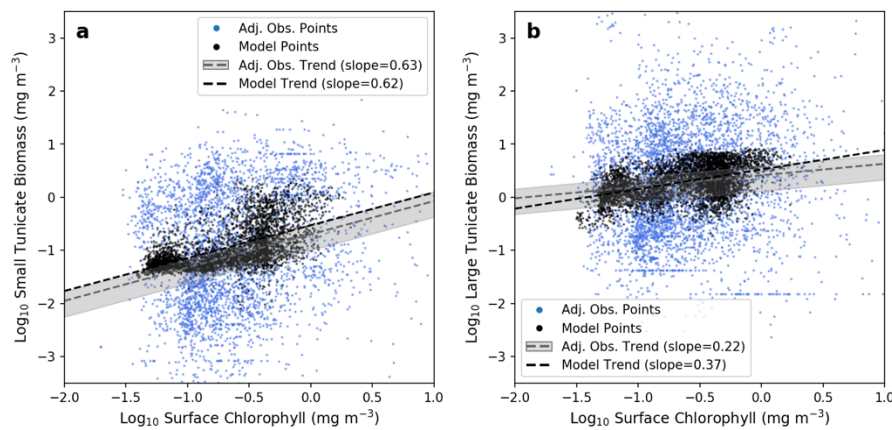


Figure S5. Biomass chlorophyll scaling for small (a) and large (b) tunicates, using daily output from the GZ-COBALT model, showing a randomly selected day within the growing season from the last year of the model simulation (2007). See also the caption in Fig. 6 for more details.

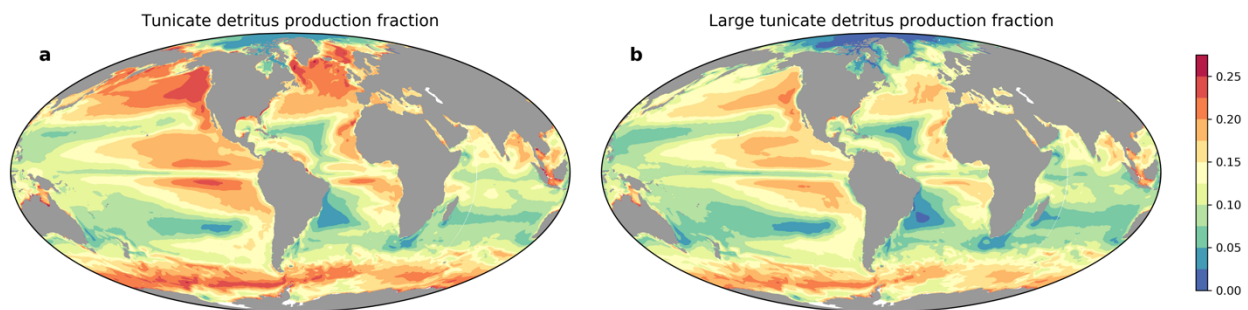


Figure S6. Fraction of late summertime detritus production in the top 100 m from (a) all tunicates, and (b) large tunicates only. Late summer is defined as July-September in the Northern Hemisphere, and January-March in the Southern Hemisphere.

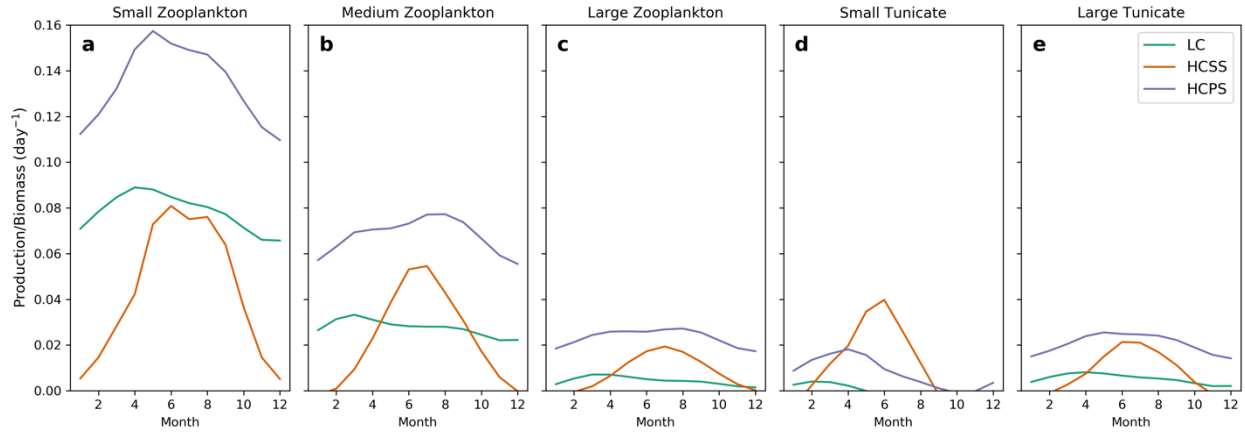


Figure S7. Mean daily Production/Biomass (P/B , d^{-1}) ratios for small zooplankton (a), medium zooplankton (b), large zooplankton (c), small tunicates (d), and large tunicates (e). Months in the Southern Hemisphere are shifted such that Austral summer occurs during months 6-8, and Austral winter occurs during months 12, 1, and 2.